An anisotropic elastoplastic constitutive model for large strain analysis of fiber reinforced composite materials

E. Car *, S. Oller, E. Oñate

E.T.S. Ingenieros de Caminos, Canales y Puertos, Universidad Politécnica de Catalunya, Módulo C1 Campus Norte, 08034 Barcelona, Spain

Abstract

In this work a generalized anisotropic elastoplastic constitutive model for the large strain analysis of fiber-reinforced composite materials in the frame of the mixing theory and the finite element method is presented. The isotropic equivalent formulation proposed assumes the existence of a fictitious isotropic space where a mapped fictitious problem is solved. Both real anisotropic and fictitious spaces are related by means of linear fourth-order transformation tensors that contain the complete information about the real anisotropic material. Details of the numerical implementation of the model into a non-linear or large strain finite element solution scheme are provided. Application examples showing the performance of the model for analysis of fiber reinforced composite materials are given. © 2000 Elsevier Science S.A. All rights reserved.

1. Introduction

The use of composite materials in structures has significantly increased during the past few years. This trend is mainly due to the fact that composite materials have properties which are very different from conventional isotropic engineering materials.

Composite materials present high strength to weight and high stiffness to weight ratio, are corrosion resistant, thermally stable and are well suited for structures in which weight is a fundamental variable in the design process. Structural components requiring high stiffness and strength, impact resistance, complex shape and high volume production are suitable candidates to be manufactured using composite materials. This explains why aerospace, automotive and marine industries have taken advantage of the special characteristics of these materials [1,30]. Components manufactured with composite materials are tough and durable, exceeding in many occasions the performance of metal parts.

In the redesign process of a structural component using composite materials, simple replacement of the component is not enough. Due to the special characteristics of these materials (high anisotropy and high strength ratio between matrix and fibers) the redesign of the component is necessary. Furthermore, analytical techniques for components manufactured with composite materials are entirely different from conventional methods of analysis used for isotropic materials and require specialist knowledge. The design process of components made up of composite materials is nowadays mostly based on empirical methods. The absence of numerical simulation tools for the non-linear analysis of the behavior of composite materials is observed in the literature.

---

* Corresponding author.
  E-mail address: car@cimne.upc.es (E. Car).

Several attempts using the finite element method (FEM) for the analysis and design of composite material components have been carried out in the past few years. The correlation between analytical and measured results is deficient [1,15]. The inability to simulate the behavior of highly non-linear anisotropic materials is the main problem with conventional FEM codes. This is extremely important in fiber-reinforced materials, which are strongly anisotropic.

To simulate the non-linear constitutive behavior of composite materials, it is necessary to consider many of their relevant features such as: (a) high anisotropy with permanent directional strains; (b) existence of several compounding substances; (c) one-directional plastic flow of fibers; (d) debonding, leading to loss of kinematic compatibility; (e) local buckling; (f) tendency of the fibers to arrange in the direction of the higher stress; and (g) large strains. All of these phenomena produce loses in the global strength and stiffness and are mainly responsible for the non-linear behavior of composite materials.

A general constitutive model for composite materials is proposed in this work. The model takes into account the relevant characteristics of the behavior of composite materials by combining the mixing theory with a general anisotropic elastoplastic constitutive model. A new procedure for treating anisotropy effects by means of an equivalent isotropic formulation is presented. The implementation of the model in a general non-linear finite element solution scheme is straightforward and some examples of the application are shown.

The layout of the paper is the following. In Section 2 an overview of different constitutive models for composite materials is given. A constitutive model based on the mechanics of a continuum medium for each point of the solid is used in this work. Section 3 describes the mixing theory chosen where the proposed anisotropic elastoplastic constitutive model is implemented. The behavior of composite materials assumes that each compound participates in the whole composite in the same volume proportion and with independent constitutive laws: elastic, elastoplastic, etc. In Section 4 the anisotropic elastoplastic constitutive model in large strains proposed to simulate the reinforcement phase is detailed. Section 5 describes the implementation of the constitutive model in the context of the mixing theory. In Section 6 details of the numerical implementation of the model into a general non-linear, large strain finite element solution scheme are provided. In Section 7 application examples showing the performance of the model for the analysis of carbon-epoxy fiber-reinforced composite structures are given.

2. Constitutive models for composite materials

Micro- and macro-models constitute the alternatives to study the mechanical behavior of composite materials. Micro-models focus on the study at the micro-mechanical level of the interatomic bounding and on the integrity of the composite beyond the damage point limit [24]. Although micro-models are quite expensive for practical purposes they can be successfully used for modeling the behavior of composite materials.

Macro-models express the whole composite behavior as that of a single material. Most macro-mechanical models are based on the mixing theory. This theory allows to study the behavior of composite materials as a combination of individual compounds each one with its own constitutive law satisfying an appropriate closing equation. This equation establishes the inter-material kinematic conditions. In this work perfect compatibility between the different compounds is assumed.

An alternative procedure used for the analysis of composite materials is the *homogenization method* [12,34,37,38]. This method has been typically used to analyze materials made up with periodic characteristics. Basically it consists of finding the solution of a cell that governs the properties of the composite. This methodology was used by Larson [16] for the study of the transport of neutrons in a non-homogeneous medium. Len'e and Leguilllon [18] and Len'e [17] used this method for the computation of the properties of a material made up of linear elastic components. The homogenization method is not satisfactory for the analysis of long fiber-reinforced composites due to the high computational costs.

The PAM-FISS code [7,36] used a bi-phase constitutive model assuming a fragile behavior of the material. The strength and stiffness of a composite are computed by adding the effect of an orthotropic matrix material and a unidimensional fiber. Matrix and fibers may have different rheological constitutive laws and can fail independently therefore simulating a fragile material. With the objective to capture cracks, fracture

mechanics is used. This methodology requires re-meshing techniques which lead to considerable computational cost.

Ali [1] treats composite materials as a stack of plies with different orientations of the principal materials directions of each plie. In the analysis he considers that each sheet presents an orthotropic linear elastic behavior. Haug et al. [11] have used the PAM-FISS bi-phase model assuming that both the matrix and fibers have a behavior characterized by a degradation of stiffness modeled by a damage constitutive law.

In this work, the non-linear behavior of composite materials is modeled by means of the mixing theory acting on a general anisotropic elastoplastic constitutive model formulated in large strains. The anisotropic elastoplastic constitutive model is considered one of the "base" models which can be included in the mixing theory. In Section 3 the characteristics of the mixing theory used are described.

3. Mixing theory – general definition

Composite materials are made of substances of inorganic or organic types. Their state of atomic balance depends on the different interatomic bonds giving place to amorphous or crystalline materials.

The mechanical characteristics of these materials result from their intrinsic properties (macroscopic structure, bond type, crystalline structure, etc.). Material behavior is also influenced by extrinsic properties such as: characteristic of the production process, microporous size and distribution, microcracks, initial stress states, etc.

The behavior of the composite is a function of the proportion of the total volume and morphologic distribution of the compounding substances.

Mixing theory is considered adequate to simulate the behavior of composite materials. This theory is the appropriate one to explain the behavior of a point of a composite based on the physical–mathematical structure of the mechanics of a continuum. Mixing theory is based on the principle of interaction of the compounding substances that constitute the material with the following hypotheses: (i) in each infinitesimal volume of a composite material participate a finite number of compounding substances; (ii) each substance participates in the behavior of the composite in the same proportion as its volumetric participation; (iii) all compounds have the same strains (closing equation or compatibility concept); (iv) the volume occupied by each compound is much smaller than the total volume of the composite.

The second hypothesis implies a homogeneous distribution of all substances in a certain region of the composite. The interaction between the different compounding substances, each one with their own constitutive ("base") model, yields the behavior of the composite which depends on the percentage volume occupied by each substance and their distribution in the composite.

Trusdell and Toupin [39] studied the mixing theory providing the background of the work of Ortiz and Popov [31]. The results obtained by Trusdell also constitute the base of the work of Green and Naghdi [10] and Ortiz and Popov [32] for bi-phase materials. The model presented here is a more general one and it allows to represent the non-linear constitutive behavior of a material made up of *n* anisotropic phases undergoing large strains.

3.1. The closing equation

Classic mixing theory is based on the combination and interaction of the basic substances that make up composite materials [10,29,32,39]. It also assumes that in each material point all the component substances contribute at the same time and with their own constitutive law in the assigned volume proportion. This allows to combine materials with different constitutive behavior (i.e. elastic, elastoplastic, elastobrittle, elastodamage, etc.).

In this work it is assumed that all phases in the mixture have the same strain field. This assumption is valid in the absence of atomic diffusion. The atomic diffusion phenomena take place at high temperatures. In this analysis, a moderate temperature below melting point is considered. The strain compatibility condition must be fulfilled in the referential and updated configurations for each phase. In the updated configuration the condition can be written as [23,39]

$$e_{ij} \equiv (e_{ij})_1 = (e_{ij})_2 = \cdots = (e_{ij})_n. \tag{1}$$

The Almansi's strain tensor can be written as

$$e_{ij} = \frac{1}{2}\left[g^{ij} - (b_{ij})^{-1}\right], \tag{2}$$

where $\mathbf{b} = \mathbf{F}\mathbf{F}^{\mathrm{T}}$ is the *left Cauchy–Green strain tensor*, g_{ij} is the spatial metric tensor given by

$$g_{ij} = I_{ij} = \delta_{ij}\begin{cases} 0 & \text{if } i \neq j, \\ 1 & \text{if } j = j \end{cases} \tag{3}$$

and $\mathbf{F}$ is the deformation gradient, which can be computed as

$$F_{iJ} = \frac{\partial x_i}{\partial X_J}. \tag{4}$$

In the referential configuration the closing equation proposed is

$$E_{IJ} \equiv (E_{IJ})_1 = (E_{IJ})_2 = \cdots = (E_{IJ})_n, \tag{5}$$

where the Green–Lagrange strain tensor is defined as

$$E_{IJ} = \frac{1}{2}(C_{IJ} - G_{IJ}), \tag{6}$$

where $\mathbf{G}$ is the material metric tensor, defined as

$$G_{IJ} = I_{IJ} = \delta_{IJ}\begin{cases} 0 & \text{if } I \neq J, \\ 1 & \text{if } I = J \end{cases} \tag{7}$$

and $\mathbf{C} = \mathbf{F}^{\mathrm{T}}\mathbf{F}$ is the right Cauchy–Green strain tensor. The relationship between Almansi's and Green–Lagrange strain tensors is shown in Appendix A.

Taking into account the definition of the right Cauchy–Green deformation tensor and Eq. (5), the closing equation is obtained in terms of the deformation gradient as

$$\mathbf{F} = \mathbf{F}_1 = \mathbf{F}_2 = \cdots = \mathbf{F}_n. \tag{8}$$

It is important to note that the strain compatibility condition chosen holds only for materials with parallel behavior. The above closing equation is therefore not valid for composites with short fibers reinforcement and in this case a correction in the properties of each compound is needed to maintain the same closing equation.

3.2. The free energy function

Composite materials that fulfill Eqs. (1) and (5) also satisfy the basic condition of additivity of the free energy of their components [39]. In the updated configuration this can be expressed as

$$m\psi(\mathbf{e}^{\mathrm{e}}, \theta, \alpha^m) = \sum_{c=1}^{n} k_c m_c \psi_c\left[\mathbf{e}, (\mathbf{e}^{\mathrm{p}})_c, \theta, \alpha_c^m\right], \tag{9}$$

where m and m_c are the density of the composite and of each of the phases in the updated configuration, respectively, ψ_c the free energy corresponding to each one of the compounding substances of the mixture, k_c the volumetric participation coefficient, $(\mathbf{e}^{\mathrm{p}})_c$ the plastic deformation of each phase and α_c^m are the internal variables of each phase which define the physical behavior of the phase.

The mixing theory used here is based on the principle that all the substances contribute to the behavior of the composite proportional to the relative volume that they occupy. The volumetric participation coefficient is defined as

$$k_c = \frac{\mathrm{d}V_c}{\mathrm{d}V_0}, \tag{10}$$

where V_c is the volume of each phase and V_0 is the total volume of the composite.

The mass conservation law establishes that

$$\frac{\mathrm{d}v}{\mathrm{d}V} = \det\mathbf{F} = J, \tag{11}$$

where v and V are the volumes in the updated and referential configurations, respectively. The relation between the volume in the updated and reference configurations for each phase can therefore be expressed by

$$\frac{\mathrm{d}v_c}{\mathrm{d}V_c} = J. \tag{12}$$

Substituting Eq. (12) into (10) gives

$$k_c = \frac{1}{J}\frac{\mathrm{d}v_c}{\mathrm{d}V_0} = \frac{\mathrm{d}v_c}{\mathrm{d}v_0}, \tag{13}$$

where v_0 is the total volume of the composite in the updated configuration. Eq. (13) shows that the volumetric participation coefficient remains constant in both updated and reference configurations.

The volumetric participation coefficient of each phase should satisfy the following condition:

$$\sum_{c=1}^{n} k_c = 1. \tag{14}$$

Mixing theory is only valid in case all the phases of the composite material are compressible or incompressible. In the presence of compressible and incompressible phases the closing equation does not hold as the incompressible phases do not admit a state of volumetric strains compatible with the compressible phases. This situation violates the strain compatibility condition.

3.3. Constitutive equation

The stress state of the composite is obtained starting from a hyperelastic model satisfying the dissipation condition of the second principle of thermodynamics, i.e.

$$\boldsymbol{\sigma} = m\frac{\partial\psi}{\partial\mathbf{e}} = \sum_{c=1}^{n} k_c m_c \frac{\partial\psi_c}{\partial\mathbf{e}} = \sum_{c=1}^{n} k_c m_c (\boldsymbol{\sigma})_c. \tag{15}$$

The tangent constitutive tensor of the composite is given by

$$\mathbf{c}^{\mathrm{T}} = \frac{\partial^2\psi}{\partial\mathbf{e}\otimes\partial\mathbf{e}} = \sum_{c=1}^{n} k_c(\mathbf{c}^{\mathrm{T}})_c, \tag{16}$$

where $(\mathbf{c}^{\mathrm{T}})_c$ is the anisotropic tangent constitutive tensor of each phase. The relationship between the constitutive tensors in the reference and updated configurations are shown in Appendix A.

Fig. 1 shows a schematic flow diagram for the non-linear solution of a multiphase material. It can be seen that each phase can have its own constitutive model and is independent of other phases.

4. Anisotropic elastoplastic model for a single phase

The constitutive model presented in this section is one of the "base" models which can be introduced in the mixing theory previously presented. This model is adequate to simulate the non-linear constitutive behavior of highly anisotropic materials.
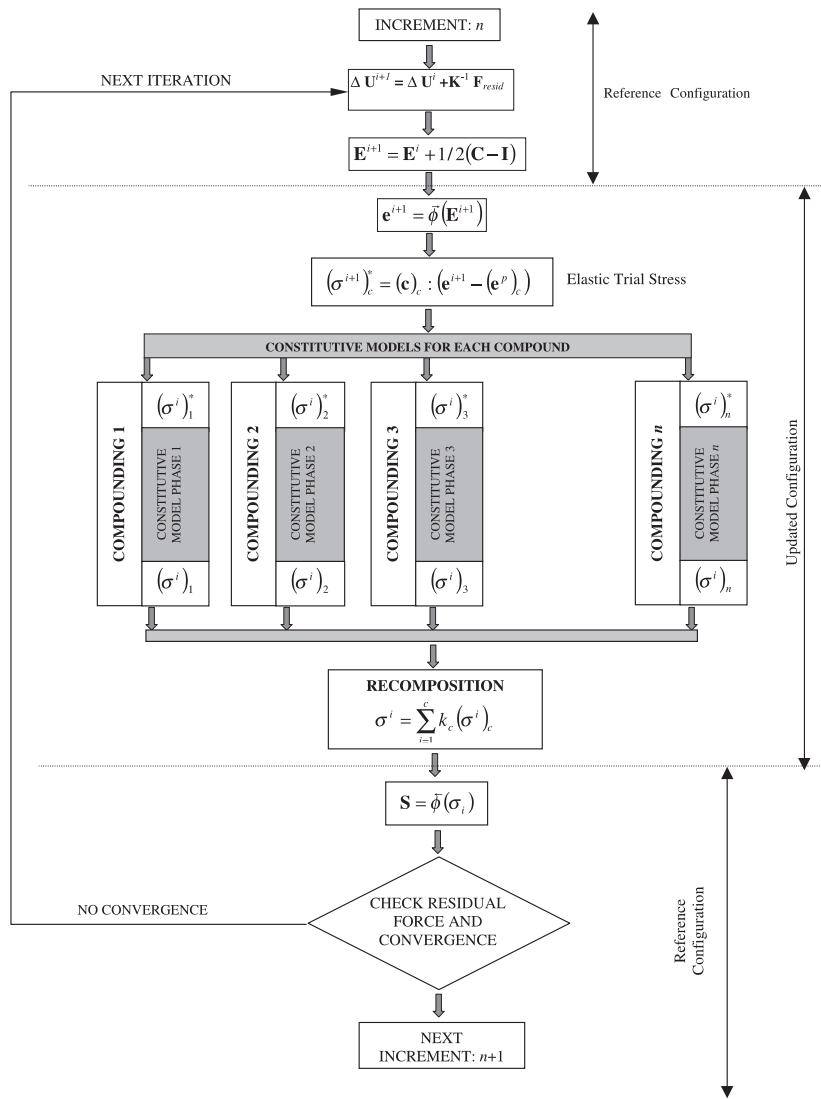
Fig. 1. Schematic flow diagram for the non-linear solution of a multiphase material formulated in the reference and updated configurations.

Modeling the behavior of an elastic anisotropic solid does not present big difficulties. In this case, it is possible to use the general elasticity theory [14,22,33], etc.

The formulation of a constitutive law adequate to simulate the non-linear behavior of orthotropic or anisotropic solids is a problem of higher complexity. The first attempts to formulate yield functions for orthotropic materials were due to Hill who was able to extend the isotropic Von Mises model to the orthotropic case [13]. The main limitation of this theory is the impossibility of modeling materials that present a behavior which not only depends on the second invariant of the stress tensor, i.e. the case of geomaterials or composite materials.

The anisotropic theory presented here is based on the ideas proposed by Betten [2,3] and uses the concept of *mapped stress tensor*. This concept makes it possible to use the advantages and algorithms of the well-known isotropic formulations; it consequently has many computational advantages.

In previous works the authors have developed a generalization from the isotropic plasticity theory to the anisotropic case [27,28]. The basic idea consists in modeling the behavior of a solid in the *real anisotropic space* through an ideal solid in a *fictitious isotropic space*. The main hypothesis is that the elastic strains are the same in both spaces, which introduces a limitation in the anisotropic mapped theory. This limitation

emanates from the necessary proportionality between the strength limit and the elasticity modulus for each material direction.

The constitutive model presented in this work is a generalization of the classical plasticity theory and it is useful to simulate high anisotropic materials, such as fiber-reinforced composites.

All the information on the material anisotropy is contained in fourth-order transformation tensors relating the stresses and strains in the real (anisotropic) and fictitious (isotropic) spaces. The parameters which define the transformation tensors can be found from adequate experimental tests. The constitutive model in the fictitious isotropic space is defined using the same yield function, plastic potential and integration algorithms developed for standard isotropic materials.

4.1. Yield and potential function

The elastic free energy is defined in terms of a simple quadratic potential. This assumption restraints the validity of the model to the small elastic strain range, whereas large plastic strains can be tackled with [8,19].

The yield and potential functions are defined in the updated configuration in the following way:

$$\text{Yield function}: f\left(\boldsymbol{\sigma}; \alpha_\sigma^m\right) = 0,$$
$$\text{Potential function}: g\left(\boldsymbol{\sigma}; \alpha_\sigma^m\right) = K, \tag{17}$$

where $\boldsymbol{\sigma}$ is the Cauchy stress tensor.

The yield and plastic potential functions are isotropic if the invariance conditions

$$f\left(a_{ip}a_{jq}\sigma_{pq}; \alpha_\sigma^m\right) = f\left(\sigma_{pq}; \alpha_\sigma^m\right) = 0 \tag{18}$$
$$g\left(a_{ip}a_{jq}\sigma_{pq}; \alpha_\sigma^m\right) = g\left(\sigma_{pq}; \alpha_\sigma^m\right) = K \tag{19}$$

are satisfied for any orthogonal transformation $a_{ik}a_{jk} = \delta_{ij}$ where a_{ij} is a unit diagonal tensor and δ_{ij} is the Kronecker tensor.

4.2. Space transformation

Traditional procedures to obtain the constitutive equations for anisotropic elastoplastic materials are based on the description of a yield and plastic potential surfaces in terms of the characteristic properties of the material. Satisfying the invariance conditions are in these cases difficult.

A procedure that guarantees satisfying the invariance conditions consists of defining the properties of the real anisotropic solid in terms of a fictitious isotropic solid through a linear relationship between the real and fictitious stresses spaces [4,26] (see Fig. 3)

$$\overline{\sigma}_{ij} = a^\sigma_{ijkl}\sigma_{kl}. \tag{20}$$

From Eq. (20)

$$\overline{\sigma}_{ij}(\sigma_{kl})^{-1} = a^\sigma_{ijkl}. \tag{21}$$

In the above σ_{kl} and $\overline{\sigma}_{ij}$ are the stress tensors in the real anisotropic and fictitious isotropic spaces, respectively, and a^σ_{ijkl} is a fourth-order tensor called *space transformation tensor*, which relates the stress in the real and fictitious spaces. In the following $\overline{(\cdot)}$ and $(\cdot)$ denote variables in the fictitious isotropic space and the real anisotropic space, respectively. The space transformation tensor is defined in the updated configuration as

$$a^\sigma_{ijkl} = \overline{f}_{ij}(f_{kl})^{-1}, \tag{22}$$

where $\overline{f}_{ij}$ and f_{kl} are the yield strengths of the material in the isotropic and anisotropic spaces, respectively.

The relationship between Almansi's elastic strains in both spaces is defined as

$$\overline{e}^e_{ij} = a^e_{ijkl}e^e_{kl}. \tag{23}$$

This assumption implies non-uniqueness of elastic strains when the change of space is produced. In Eq. (23) a^{e}_{ijkl} is the fourth-order strain transformation tensor. This tensor can be derived from Eq. (20) as follows:

$$
\begin{aligned}
a^{\sigma}_{ijkl} &= \overline{\sigma}_{ij}(\sigma_{kl})^{-1} = \left(\overline{c}_{ikrs}\overline{e}^{\mathrm{e}}_{rs}\right)\left(c_{jlmn}e^{\mathrm{e}}_{mn}\right)^{-1} \\
&= \overline{c}_{ikrs}\overline{e}^{\mathrm{e}}_{rs}\left(e^{\mathrm{e}}_{mn}\right)^{-1}\left(c_{jlmn}\right)^{-1} \\
&= \overline{c}_{ikrs}a^{\mathrm{e}}_{rsmn}\left(c_{jlmn}\right)^{-1}
\end{aligned}
\tag{24}
$$

and hence

$$
a^{\mathrm{e}}_{rsmn} = \left(\overline{c}_{ikrs}\right)^{-1}a^{\sigma}_{ijkl}c_{jlmn},
\tag{25}
$$

where $\overline{c}_{ikrs}$ and c_{jlmn} are the constitutive tensors in the fictitious and real spaces and relating stresses and strains in the standard manner as

$$
\sigma_{ij} = c_{ijkl}\varepsilon_{kl},
\tag{26}
$$
$$
\overline{\sigma}_{ij} = \overline{c}_{ijkl}\varepsilon_{kl}.
\tag{27}
$$

Note that c_{ijkl} includes the actual properties of the material. The choice of $\overline{c}_{ijkl}$ can be arbitrary and for this purpose the property of any known material can be chosen.

The relationship between the constitutive tensor in the real and the fictitious spaces is deduced from Eq. (24) as

$$
c_{jlmn} = \left(a^{\sigma}_{ijkl}\right)^{-1}\overline{c}_{ikrs}a^{\mathrm{e}}_{rsmn}.
\tag{28}
$$

Note that the anisotropic constitutive tensor $\mathbf{c}$ is expressed in a local reference system. This means that prior to the derivation of $\mathbf{a}^{\mathrm{e}}$ and $\mathbf{a}^{\sigma}$ it is necessary to transform of $\mathbf{c}$ to a global reference system, i.e.,

$$
c_{ijkl} = R_{irjs}\left(c_{rspq}\right)_{\mathrm{loc}}R_{kplq},
\tag{29}
$$

where $(c_{rspq})_{\mathrm{loc}}$ is the local anisotropic constitutive tensor. The rotation tensor is defined as

$$
R_{ijkl} = r_{ik}r_{jl},
\tag{30}
$$

where $r_{ik} = \cos((\vec{e}_i)_{\mathrm{glob}}, (\vec{e}_j)_{\mathrm{loc}})$ and $\vec{e}_i$ is the unit vector corresponding to the kth component of the global reference coordinate system chosen. The rotation tensor $\mathbf{R}$ takes into account the angles between the local principal directions of the anisotropic material and those of the global coordinate system.

The transformation of Eq. (20) leads to changes in the shape of the yield surface. This can be observed in Fig. 2 for different yields functions. The space mapping allows to represent appropriately high anisotropic yield and potential surfaces, such as in the case of fiber-reinforced composites where the relationship $r = \overline{\sigma}_{ii}/\sigma_{ii}$ is large. Note in Fig. 2 the loss of strength in a given direction for the case of the Von Mises associate plasticity yield function, while in the normal direction the plastic flow increases in the same proportion.

4.3. Constitutive equation

In this section the free energy function for each of the anisotropic phases of a composite is derived. This function is then used to define the stress state from Eq. (15).

4.3.1. Basic aspects

The constitutive equation for an anisotropic material is obtained by writing the dissipation of an iso-thermic elastoplastic process in the real anisotropic space. The dissipation expression is obtained taking into account the first and second principles of thermodynamics.

The first principle postulates the balance of the energy, demanding the conservation of the total internal energy of the system. The local Eulerian form of the energy rate can be expressed by [19,21].
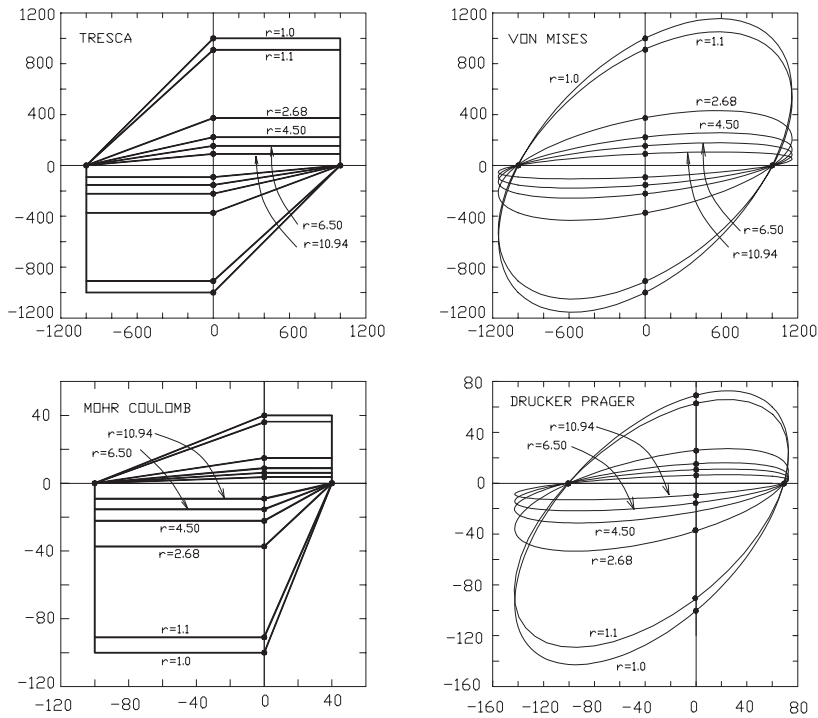
Fig. 2. Changes in the shape of several yield functions. r is the relationship between the fictitious isotropic and the real anisotropic yield stresses.

$$m\dot{\psi} = \boldsymbol{\sigma} : \mathbf{d} + mr - \operatorname{div}(\mathbf{q}) - m\dot{\eta}\theta - m\eta\dot{\theta}, \tag{31}$$

where $\dot{\psi}$ is the internal specific energy, $\boldsymbol{\sigma}$ the Cauchy stress tensor, $\mathbf{d}$ the velocity gradient, r the specific internal source of heat, $\mathbf{q}$ the conductivity heat flow and ψ is the Helmholtz free energy density.

The second principle establishes that for an irreversible process the change in the internal production of entropy should be bigger or the same than the change of introduced entropy [21,25]. This gives the specific local dissipation as

$$\Xi = -\dot{\theta}\eta - \dot{\psi} + \left(\frac{\boldsymbol{\sigma} : \mathbf{d}}{m}\right) - \frac{1}{\theta m}q \cdot \nabla\theta. \tag{32}$$

4.3.2. Helmholtz's free energy function definition

In the definition of Helmholtz's free energy, it is not correct to use as a free variable the elastic Green–Lagrange strain tensor as this is affected by the plastic flow through the plastic component of the deformation gradient $\mathbf{F}^{\mathrm{p}}$. A more convenient form of Helmhotlz's free energy is

$$\psi = \psi(\mathbf{e}^{\mathrm{e}}; \theta; \alpha_i), \tag{33}$$

where θ is the absolute temperature, $\mathbf{e}^{\mathrm{e}}$ the Almansi's strain tensor and α_i is a set of internal plastic variables.

4.3.3. Hypothesis of uncoupled elasticity

The hypothesis of uncoupled elasticity transforms Eq. (33) into

$$\psi(\mathbf{e}^{\mathrm{e}}; \theta; \alpha) = \psi^{\mathrm{e}}(\mathbf{e}^{\mathrm{e}}; \theta) + \psi^{\mathrm{p}}(\alpha_i; \theta). \tag{34}$$

This assumption is based on the fact that the necessary energy levels to distort the crystalline net, responsible for the elastic strains, are different from the necessary energy levels for the intercrystalline slip. This splitting has been used by several authors and is the base of different computational models [8,9,19,20,25].

The free variables of the problem are the temperature θ and the elastic part of Almansi's strain tensor which is defined as

$$\mathbf{e}^e = \mathbf{e} - \mathbf{e}^p = \frac{1}{2}\left(\mathbf{I} - \mathbf{b}^{-1}\right) - \int_0^t \dot{\mathbf{e}}^p \, dt, \tag{35}$$

where $\mathbf{e}^p$ is the plastic strain in the updated configuration, $\mathbf{b}$ the left Cauchy–Green tensor and $\dot{\mathbf{e}}^p$ is the rate of change of plastic strains in the updated configuration.

4.3.4. Dissipation expression

The rate of change of the free energy function is given by

$$\dot{\psi} = \frac{\partial \psi}{\partial \mathbf{e}^e} \mathbf{d}^e + \frac{\partial \psi}{\partial \theta} \dot{\theta} + \frac{\partial \psi}{\partial \alpha_i} \dot{\alpha}_i, \tag{36}$$

where $\mathbf{d}^e = L_v(\mathbf{e}^e)$ is the rate of change of the elastic part of the strains. The term L_v denotes the standard Lee derivative (see Appendix A). Substituting Eq. (36) into (32) gives the expression of the dissipation as

$$\Xi = \left[\boldsymbol{\sigma} : \mathbf{d} - \frac{\partial \psi}{\partial \mathbf{e}^e} \mathbf{d}^e m\right] - m\dot{\theta}\left[\frac{\partial \psi}{\partial \theta} - \eta\right] - m\frac{\partial \psi}{\partial \alpha}\dot{\alpha} - \frac{1}{\theta}\mathbf{q} \cdot \nabla\theta \geqslant 0. \tag{37}$$

Taking into account the additive decomposition of the velocity gradient tensor $\mathbf{d} = \mathbf{d}^e + \mathbf{d}^p$ [8] Eq. (37) becomes

$$\Xi = \left[\boldsymbol{\sigma} - m\frac{\partial \psi}{\partial \mathbf{e}^e}\right] : \mathbf{d}^e - m\dot{\theta}\left[\frac{\partial \psi}{\partial \theta} - \eta\right] + \boldsymbol{\sigma} : \mathbf{d}^p - m\frac{\partial \psi}{\partial \alpha}\dot{\alpha} - \frac{1}{\theta}\mathbf{q} \cdot \nabla\theta \geqslant 0, \tag{38}$$

Eq. (38) is known as the Clasius–Duhem inequality. In continuum mechanics this inequality must be satisfied for every possible process, since $\mathbf{d}$ and $\dot{\theta}$ represent arbitrary temporary changes of the free variables of the problem. Eq. (38) imposes restrictions in the form of the constitutive equations and it is satisfied only if the multipliers of $\mathbf{d}^e$ and $\dot{\theta}$ are null. This allow to define the constitutive equation in general form as

$$\boldsymbol{\sigma} = m\frac{\partial \psi}{\partial \mathbf{e}^e}; \quad \eta = \frac{\partial \psi}{\partial \theta}. \tag{39}$$

The expression of the free energy function is derived in Section 4.3.5.

4.3.5. Free energy expression. Special case: small elastic strains and isothermal state

Composite materials are usually subjected to small elastic strains. Thus the elastic part of the deformation gradient $\mathbf{F}^e$ tends to unity and the elastic part of the left Cauchy–Green tensor $(\mathbf{b}^e)^{-1}$ tends to the spatial metric tensor $\mathbf{g}$. In this case the distinction between intermediate and deformed configurations is irrelevant.

However, the plastic strains continue being finite and therefore it is necessary to keep the presence of the right Cauchy–Green tensor $\mathbf{C}$ in the material expression of the constitutive model to preserve the physical meaning of the model.

For the case of small elastic strains it is enough to characterize the elastic component of the free energy by means of a quadratic function of the elastic part of Almansi's strain tensor, i.e.

$$\psi^e = \frac{1}{2m}\mathbf{e}^e : \mathbf{c} : \mathbf{e}^e. \tag{40}$$

The expression of the free energy function can be rewritten taking into account the hypothesis of uncoupled elasticity (Eq. (34)), the expression of the elastic part of the free energy (Eq. (40)) and the relationship between the constitutive tensors in the real and fictitious spaces (Eq. (28)). This gives

$$\psi = \frac{1}{2m}(\mathbf{e}^e : \mathbf{c} : \mathbf{e}^e) + \psi^p \tag{41}$$

$$= \frac{1}{2m}\mathbf{e}^e : \left[(\mathbf{a}^\sigma)^{-1} : \overline{\mathbf{c}} : (\mathbf{a}^e)\right] : \mathbf{e}^e + \psi^p(\alpha). \tag{42}$$

The constitutive equation in the real anisotropic space is obtained substituting Eq. (42) into (39), i.e.,

$$\boldsymbol{\sigma} = m\frac{\partial\psi}{\partial\mathbf{e}^e} = \left[(\mathbf{a}^\sigma)^{-1} : \overline{\mathbf{c}} : (\mathbf{a}^e)\right] : \mathbf{e}^e = \left[(\mathbf{a}^\sigma)^{-1} : \overline{\mathbf{c}}\right] : \overline{\mathbf{e}}^e = (\mathbf{a}^\sigma)^{-1} : \overline{\boldsymbol{\sigma}}, \tag{43}$$

Eq. (43) shows that the stresses in the real anisotropic space are obtained by transformation of the stresses in the fictitious isotropic stress state through $(\mathbf{a}^\sigma)^{-1}$.

4.4. Flow rule. Evolution law for the internal variables

The rate expression of the plastic strain is defined by

$$\mathbf{d}^p = \dot{\mathbf{e}}^p = \dot{\lambda}\frac{\partial g}{\partial\boldsymbol{\sigma}}. \tag{44}$$

All the relevant information on the material anisotropy properties is contained in the two fourth-order tensors $\mathbf{a}^\sigma$ and $\mathbf{a}^e$. The expression of the plastic potential function for the anisotropic solid is written in terms of these tensors and the Cauchy stress tensor as

$$g(\boldsymbol{\sigma};\alpha) = \overline{g}(\boldsymbol{\sigma};\mathbf{a}^\sigma;\alpha) = \overline{g}(\overline{\boldsymbol{\sigma}};\alpha) = K. \tag{45}$$

Substituting Eq. (45) into (44) the rate of the plastic Almansi strains is

$$\dot{\mathbf{e}}^p = \dot{\lambda}\frac{\partial g}{\partial\boldsymbol{\sigma}} = \dot{\lambda}\frac{\partial\overline{g}}{\partial\overline{\boldsymbol{\sigma}}} : \frac{\partial\overline{\boldsymbol{\sigma}}}{\partial\boldsymbol{\sigma}} = \dot{\lambda}\frac{\partial\overline{g}}{\partial\overline{\boldsymbol{\sigma}}} : \mathbf{a}^\sigma = \left(\dot{\overline{\mathbf{e}}}\right)^\sigma : \mathbf{a}^\sigma, \tag{46}$$

where $(\dot{\overline{\mathbf{e}}})^\sigma$ is the plastic flow normal to the isotropic potential function $\overline{g}$.

The evolution law of the plastic internal variables is given by

$$\dot{\alpha} = \dot{\lambda}(\mathbf{h}^i)_\sigma : \frac{\partial g}{\partial\boldsymbol{\sigma}} = \dot{\lambda}(\mathbf{h}^i)_\sigma : \frac{\partial\overline{g}}{\partial\overline{\boldsymbol{\sigma}}} : \frac{\partial\overline{\boldsymbol{\sigma}}}{\partial\boldsymbol{\sigma}} = \dot{\lambda}(\mathbf{h}^i)_\sigma : \frac{\partial\overline{g}}{\partial\overline{\boldsymbol{\sigma}}} : \mathbf{a}^\sigma, \tag{47}$$

where $(\mathbf{h}^i)_\sigma$ is a second-order tensor to be determined for each one of the i internal variables. In the simplest case of plasticity theory this tensor takes the form of the Cauchy stress tensor. In this case the evolution law of the internal variables can be written as

$$\dot{\alpha} = \dot{\lambda}\overline{\boldsymbol{\sigma}} : \frac{\partial\overline{g}}{\partial\overline{\boldsymbol{\sigma}}}. \tag{48}$$

The additivity strain concept (see Eq. (35)) allows to extend the transformation rule defined for the total strains to their plastic part, i.e.,

$$\dot{\overline{\mathbf{e}}}^p = \mathbf{a}^e : \dot{e}^p = \dot{\lambda}a^e : \frac{\partial\overline{g}}{\partial\overline{\boldsymbol{\sigma}}} : \mathbf{a}^\sigma = \mathbf{a}^e : \left(\dot{\overline{\mathbf{e}}}\right)^\sigma : \mathbf{a}^\sigma, \tag{49}$$

where $\dot{\overline{\mathbf{e}}}^p$ is the plastic strain tensor in the fictitious space.

4.4.1. Dissipation in isotropic fictitious space. Uniqueness of dissipation

In this section the invariance of the dissipation through the thermodynamic process is shown. As a consequence it is concluded that it is irrelevant to write the constitutive model in either the anisotropic or isotropic spaces.

The expression of the mechanic dissipation in the fictitious isotropic space can be written taking into account the following transformations

$$\overline{\boldsymbol{\sigma}} = \mathbf{a}^{\sigma} : \boldsymbol{\sigma}, \tag{50a}$$

$$\overline{\mathbf{e}} = \mathbf{a}^{e} : \mathbf{e}. \tag{50b}$$

The rate of change of plastic strains in the fictitious isotropic space is given by

$$\dot{\overline{\mathbf{e}}}^{p} = \dot{\lambda} \mathbf{a}^{e} : \frac{\partial \overline{g}}{\partial \overline{\boldsymbol{\sigma}}} : \mathbf{a}^{\sigma}. \tag{51}$$

Taking into account Eq. (38), the plastic dissipation in the real anisotropic space for the isothermal process is

$$\varXi_{\text{mec}} = \boldsymbol{\sigma} : \mathbf{d}^{p} - m \frac{\partial \psi}{\partial \alpha} \dot{\alpha} \geqslant 0. \tag{52}$$

The dissipated mechanical power can be written in the fictitious isotropic space by substituting in Eq. (52) the flow rule, the evolution law of the internal variables and taking into account Eqs. (50a) and (50b), i.e.

$$\boldsymbol{\sigma} : \dot{\mathbf{e}}^{p} = \left[(\mathbf{a}^{\sigma})^{-1} : \overline{\boldsymbol{\sigma}} \right] : \left[(\mathbf{a}^{e})^{-1} : \dot{\overline{\mathbf{e}}}^{p} \right] = \dot{\lambda} (\mathbf{a}^{\sigma})^{-1} : \overline{\boldsymbol{\sigma}} : (\mathbf{a}^{e})^{-1} : \mathbf{a}^{e} : \frac{\partial \overline{g}}{\partial \overline{\boldsymbol{\sigma}}} : \mathbf{a}^{\sigma} = \dot{\lambda} \overline{\boldsymbol{\sigma}} \frac{\partial \overline{g}}{\partial \overline{\boldsymbol{\sigma}}} = \overline{\boldsymbol{\sigma}} : \left(\dot{\overline{\mathbf{e}}} \right)^{\sigma}. \tag{53}$$

Substituting this expression into Eq. (52) and using Eq. (44) gives

$$\varXi_{\text{mec}} = \boldsymbol{\sigma} : \mathbf{d}^{p} - m \frac{\partial \psi}{\partial \alpha} \dot{\alpha} = \overline{\boldsymbol{\sigma}} : \left(\dot{\overline{\mathbf{e}}} \right)^{\sigma} - m \frac{\partial \psi}{\partial \alpha} \dot{\alpha} \equiv \overline{\varXi}_{\text{mec}} \geqslant 0, \tag{54}$$

Eq. (54) shows that the dissipation is an invariant of the thermodynamic process. Therefore, its value is independent of the space where it is computed.

Helmholtz's free energy in an isothermal process can be expressed in the isotropic fictitious space by

$$\overline{\psi}(\overline{\mathbf{e}}^{e}; \alpha) = \frac{1}{2m} (\overline{\mathbf{e}}^{e} : \overline{\mathbf{c}} : \overline{\mathbf{e}}^{e}) + \overline{\psi}^{p}(\alpha^{m}) \tag{55}$$

and hence the constitutive equation in the fictitious isotropic space is given by

$$\overline{\boldsymbol{\sigma}} = m \frac{\partial \overline{\psi}(\overline{\mathbf{e}}^{e}; \alpha)}{\partial \overline{\mathbf{e}}^{e}} = \overline{\mathbf{c}} : \overline{\mathbf{e}}^{e}. \tag{56}$$

Taking into account Eqs. (28) and (50b) Cauchy's stress tensor in the fictitious isotropic space is given by

$$\overline{\boldsymbol{\sigma}} = \left[\mathbf{a}^{\sigma} : \mathbf{c}^{\sigma} : (\mathbf{a}^{e})^{-1} \right] : (\mathbf{a}^{e} : \mathbf{e}^{e}) = \mathbf{a}^{\sigma} : \mathbf{c}^{\sigma} : \mathbf{I} : \mathbf{e}^{e} = \mathbf{a}^{\sigma} : \mathbf{c}^{\sigma} : \mathbf{e}^{e} = \mathbf{a}^{\sigma} : \boldsymbol{\sigma}. \tag{57}$$

The previous expression and Eq. (54) show that it is equivalent to write the constitutive model in the anisotropic real space or in the isotropic fictitious one. Obviously writing the constitutive models in the isotropic fictitious space allows to profit from the advantages and algorithms used for isotropic materials.

4.5. Tangent constitutive equation

The expression of the tangent constitutive equation is obtained by performing the temporal derivative of Eq. (43), i.e.

$$\begin{aligned} \dot{\sigma}_{ij} &= \frac{\partial \sigma_{ij}}{\partial e^{e}_{kl}} \dot{e}^{e}_{kl} \\ &= \frac{\partial \sigma_{ij}}{\partial \overline{\sigma}_{rs}} \frac{\partial \overline{\sigma}_{rs}}{\partial \overline{e}^{e}_{mn}} \frac{\partial \overline{e}^{e}_{mn}}{\partial e^{e}_{kl}} \dot{e}^{e}_{kl} \\ &= \left(a^{\sigma}_{ijrs} \right)^{-1} \overline{c}_{rsmn} a^{e}_{mnkl} \dot{e}^{e}_{kl} \\ &= \left(a^{\sigma}_{ijrs} \right)^{-1} \overline{c}_{rsmn} \left(\dot{\overline{e}}_{kl} - \dot{\overline{e}}^{p}_{kl} \right). \end{aligned} \tag{58}$$

This equation can also be obtained considering Eq. (50a) relating the Cauchy stress tensor in the fictitious and real spaces. Taking into account that the stress transformation tensor between spaces $\mathbf{a}^\sigma$ is time independent and the plastic consistency condition, the rate constitutive equation in the fictitious isotropic space is obtained as

$$\dot{\overline{\boldsymbol{\sigma}}} = (\overline{\mathbf{c}})^{\mathrm{ep}} : \dot{\overline{\mathbf{e}}}, \tag{59}$$

where $(\overline{\mathbf{c}})^{\mathrm{ep}}$ is the tangent elastoplastic constitutive tensor in the fictitious isotropic space given by

$$\overline{c}_{ijkl}^{\mathrm{ep}} = \overline{c}_{ijkl} - \frac{\left(\overline{c}_{ijrs}(\partial \overline{g}/\partial \overline{\sigma}_{rs})\right)\left((\partial \overline{f}/\partial \overline{\sigma}_{rs})\overline{c}_{rskl}\right)}{(\partial \overline{f}/\partial \overline{\sigma}_{pq})c_{pqln}(\partial \overline{g}/\partial \overline{\sigma}_{ln}) - \sum_n (\partial f^{\overline{\sigma}}/\partial \alpha_s^m)\left(h_{tu}^m\right)_{\overline{\sigma}}(\partial \overline{g}/\partial \overline{\sigma}_{tu})}. \tag{60}$$

The rate expression of Cauchy's stress tensor in the anisotropic space is obtained taking into account Eq. (50a), i.e.,

$$\dot{\sigma}_{ij} = \left(a_{ijkl}^\sigma\right)^{-1}\overline{c}_{klrs}^{\mathrm{ep}}\dot{\overline{e}}_{rs}. \tag{61}$$

Combining Eqs. (61) and (50b) leads to the final expression of the rate constitutive equation in the anisotropic solid as

$$\dot{\sigma}_{ij} = \left(a_{ijkl}^\sigma\right)^{-1}\overline{c}_{klrs}^{\mathrm{ep}}a_{rspq}^{\mathrm{e}}\dot{e}_{pq} = c_{ijpq}^{\mathrm{ep}}\dot{e}_{pq} \tag{62}$$

with

$$c_{ijpq}^{\mathrm{ep}} = \left(a_{ijkl}^\sigma\right)^{-1}\overline{c}_{klrs}^{\mathrm{ep}}a_{rspq}^{\mathrm{e}}, \tag{63}$$

Eq. (62) shows that the expression of the tangent elastoplastic anisotropic tensor is a function of the tangent elastoplastic constitutive tensor in the fictitious isotropic space through $\mathbf{a}^\sigma$ and $\mathbf{a}^{\mathrm{e}}$.

In order to simulate the constitutive behavior of highly anisotropic composite materials the constitutive model here proposed only requires the definition of the following material properties in the real and fictitious spaces:

- Real anisotropic space.
  - Initial constitutive tensor in local coordinates $\mathbf{c}_{\mathrm{local}}$.
  - Yield strength σ_{yield}.
  - Rotation tensor $\mathbf{R}$.
- Fictitious isotropic space.
  - Yield function $\overline{f}(\overline{\boldsymbol{\sigma}}, \alpha) = 0$.
  - Plastic potential function $\overline{g}(\overline{\boldsymbol{\sigma}}, \alpha) = 0$.
  - Yield strength $\overline{\sigma}_{\mathrm{yield}}$.

Fig. 3 shows the operations to be performed for an anisotropic compounding of a composite material. The first operation is to transport the strain tensor from the reference configuration to the updated configuration using a ''push forward'' operation (see Appendix A). In step 2 a trial stress $\boldsymbol{\sigma}^*$ is computed. Next the trial stresses $\boldsymbol{\sigma}^*$, the strains $\mathbf{e}$ and the constitutive tensors $\mathbf{c}$ are transported from the real anisotropic updated configuration to the fictitious isotropic space using tensors $\mathbf{a}^\sigma$ and $\mathbf{a}^{\mathrm{e}}$. In the fictitious isotropic space the yield condition must be satisfied. Otherwise an elastoplastic problem must be solved providing a new stress state $\overline{\boldsymbol{\sigma}}$ and the tangent elastoplastic constitutive tensor $(\overline{\mathbf{c}})^{\mathrm{ep}}$. In step 3 the new stress state and the tangent elastoplastic constitutive tensor must be mapped to the real anisotropic updated configuration using $(\mathbf{a}^\sigma)^{-1}$ and $(\mathbf{a}^{\mathrm{e}})^{-1}$ tensors, giving $\boldsymbol{\sigma}$ and $(\mathbf{c})^{\mathrm{ep}}$. In step 4 $\boldsymbol{\sigma}$ and $(\mathbf{c})^{\mathrm{ep}}$ are mapped to the reference anisotropic configuration. Finally the residual force is computed and a convergence check is performed.
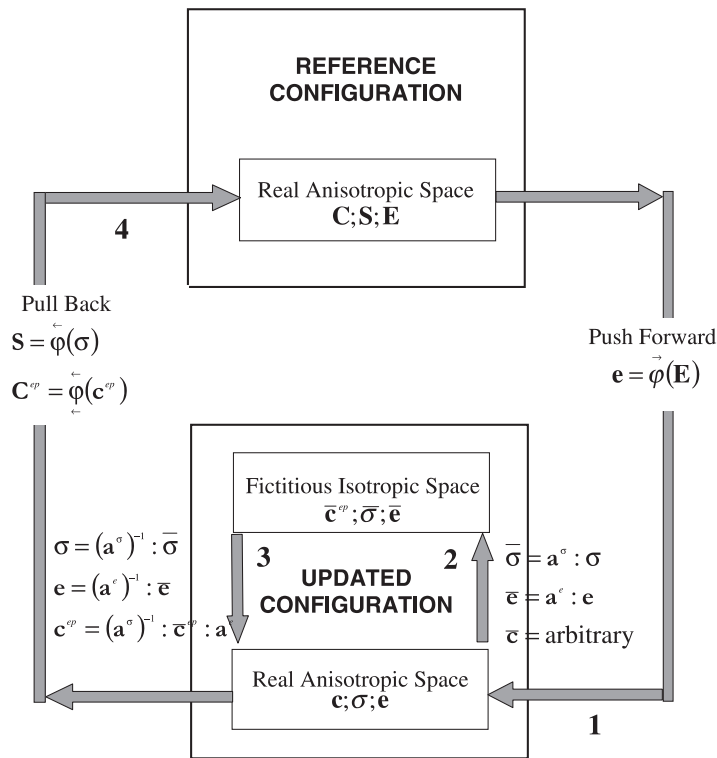
Fig. 3. Scheme of the elastoplastic anisotropic constitutive model.

4.6. Integration of the constitutive equation

A material with inelastic behavior requires the numerical integration of the constitutive equation in a discrete sequence of time steps.

The result of the integration algorithm is a non-linear function that defines the stress tensor in terms of the history of strains until the current time step. This integration algorithm allows to treat the elastoplastic problem as an equivalent elastic problem in the time step.

The tangent operator used in the linearized problem should be obtained by linearizing the response function consistently with the integration algorithm of the constitutive equation. The use of the consistent tangent operators preserves the quadratic convergence of iterative solution schemes based on Newton methods.

In the proposed constitutive model the integration of the constitutive equation is carried out in the fictitious isotropic space by means of "return mapping algorithm" using the backward-Euler scheme [5]. In the solution of elastoplastic problems that require incremental constitutive equations the consistency between the tangent operator and the integration algorithm plays a fundamental role [5,35]. In the proposed model consistent tangent operators have been used to preserve the quadratic convergence of Newton methods.

5. Composite constitutive model

The large strain anisotropic elastoplastic constitutive model presented in the previous section is one of the "base" model used in the mixing theory. In particular, in the case of fiber-reinforced composite materials a constitutive model for each phase is considered (see Fig. 4). A standard isotropic plasticity model
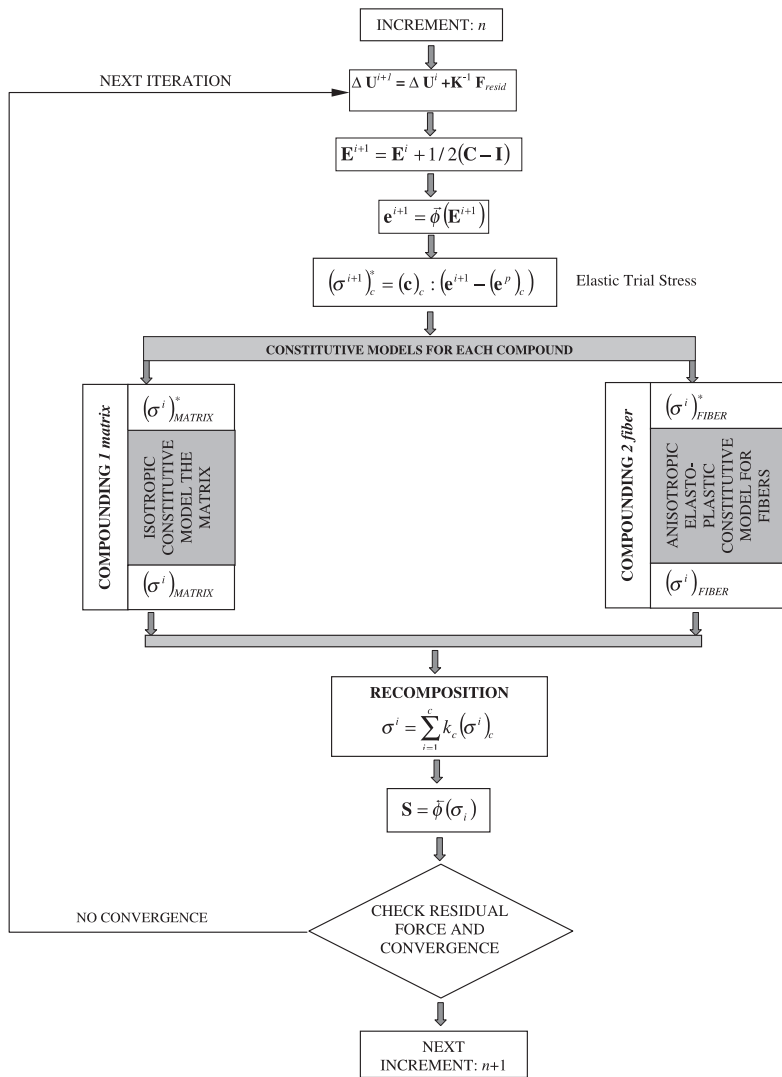
Fig. 4. Constitutive model for fiber reinforced composite materials.

has been chosen for the matrix material, whereas the behavior of the fiber reinforcement is modeled by means of the anisotropic elastoplastic model here proposed.

6. Numerical implementation of the proposed model

In this section the basic steps for the implementation of the constitutive model into a standard elasto-plastic finite element program are given.

Box 1.

Numerical implementation (1)
– Definition of the yield stress tensors in the real anisotropic space and the isotropic fictitious space for each phase of the composite material

$$\bar{\mathbf{f}}; \mathbf{f}$$

– Definition of the constitutive tensor in the real anisotropic space, of the constitutive fictitious isotropic tensor in the reference configuration and of the rotating tensor for each phase of the material

$\overline{\mathbf{c}}; (\mathbf{c})_{\mathrm{loc}}; \mathbf{R}$

– Compute the anisotropic constitutive tensor in the global coordinate system for each phase of the composite material

$\mathbf{c} = \mathbf{R} : (\mathbf{c})_{\mathrm{loc}} : \mathbf{R}$

– Definition of the mapping tensors for each phase of the composite material

$\mathbf{a}^{\sigma} = \overline{\mathbf{f}} \otimes (\mathbf{f})^{-1}; \quad \mathbf{a}^{\mathrm{e}} = (\overline{\mathbf{c}})^{-1} : \mathbf{a}^{\sigma} : \mathbf{c}$

– Compute the anisotropic and isotropic constitutive tensors from the mixing theory

$$\mathbf{c} = \sum_{c=1}^{n} k_c (\mathbf{c})_c; \quad \overline{\mathbf{c}} = \sum_{c=1}^{n} k_c (\overline{\mathbf{c}})_c$$

★ LOOP OVER LOAD INCREMENT $n = 1$, Max. Load increment
  • LOOP OVER ITERATION: $i = 1$, Max. number of iterations
    1. Compute stiffness matrix

$${}^{n}\left[K^{(e)}\right]^{i} \Rightarrow {}^{n}(K)^{i} = \mathbb{A}_{e=1}^{\mathrm{nelem}}\left[K^{(e)}\right]^{i}$$

    2. Compute strain increments in the reference configuration

$${}^{n}(\Delta U)^{i+1} = \left[{}^{n}(K)^{i}\right]^{-1} \cdot (F_{\mathrm{resid}})^{i}; \quad {}^{n}(U)^{i+1} = {}^{n}(\Delta U)^{i} + {}^{n}(\Delta U)^{i+1}$$
$${}^{n}(\mathbf{E})^{i+1} = 1/2\left(\mathbf{F}^{\mathrm{T}}\mathbf{F} - \mathbf{I}\right)$$

    3. Push-forward of the strain tensor to the updated configuration

$${}^{n}(\mathbf{e})^{i+1} = \vec{\phi}\left[{}^{n}(\mathbf{E})^{i+1}\right]$$

    4. Integration of the constitutive equation in the updated configuration
    ♣ LOOP OVER EACH PHASE OF COMPOSITE MATERIAL: $j = 1$, NCOMP
      (a) Compute elastic trial stress

$$\left[{}^{n}(\boldsymbol{\sigma}^{*})^{i+1}\right]_{c} = [\mathbf{c}]_{c} : \left[{}^{n}(\mathbf{e})^{i+1} - {}^{n}(\mathbf{e}^{\mathrm{p}})\right]$$

      (b) Transform predicted stresses to the fictitious isotropic space

$$\left[{}^{n}(\overline{\boldsymbol{\sigma}}^{*})^{i+1}\right]_{c} = [\mathbf{a}^{\sigma}]_{c} : \left[{}^{n}(\boldsymbol{\sigma}^{*})^{i+1}\right]_{c}$$

      (c) Integration of the constitutive equation

$$\left[{}^{n}(\overline{\boldsymbol{\sigma}}^{*})^{i+1}\right]_{c} \Rightarrow \left[{}^{n}(\overline{\boldsymbol{\sigma}})^{i+1}\right]_{c}$$
$${}^{n}[(\overline{\mathbf{c}})^{\mathrm{ep}}]_{c}^{i+1} = \left[\overline{\mathbf{c}} - \frac{(\overline{\mathbf{c}} : (\partial\overline{g}/\partial\overline{\boldsymbol{\sigma}})) \otimes ((\partial\overline{f}/\partial\overline{\boldsymbol{\sigma}}) : \overline{\mathbf{c}})}{(\partial\overline{f}/\partial\overline{\boldsymbol{\sigma}}) : \overline{\mathbf{c}} : (\partial\overline{g}/\partial\overline{\boldsymbol{\sigma}}) - \sum_{\mathbf{n}}(\partial\overline{f}/\partial\alpha_{\mathbf{s}}^{\mathbf{m}}) : (\mathbf{h}^{\mathbf{m}})_{\overline{\sigma}} : (\partial\overline{g}/\partial\overline{\boldsymbol{\sigma}})}\right]_{c}$$

      (d) Back transformation of stresses and tangent elastoplastic constitutive tensor to the real anisotropic space

$$\left[{}^{n}(\sigma)^{i+1}\right]_{c} = \left[(\mathbf{a}^{\sigma})^{-1}\right]_{c} : \left[{}^{n}(\overline{\sigma})^{i+1}\right]_{c}$$
$${}^{n}[(\mathbf{c})^{\mathrm{ep}}]_{c}^{i+1} = \left[(\mathbf{a}^{\sigma})^{-1}\right]_{c} : {}^{n}[(\overline{\mathbf{c}})^{\mathrm{ep}}]_{c}^{i+1} : (\mathbf{a}^{\mathrm{e}})_{c})$$

    ♣ END LOOP OVER EACH PHASE OF COMPOSITE MATERIAL

5. Compute composite stresses and constitutive tensor according to the mixing theory

$$^{n}(\sigma)^{i+1} = \sum_{i=1}^{\text{ncomp}} k_c \left[^{n}(\sigma)^{i+1} \right]_c$$

$$^{n}[(\mathbf{c})^{\text{ep}}]^{i+1} = \sum_{i=1}^{\text{ncomp}} k_c \left[^{n}[(\mathbf{c})^{\text{ep}}]^{i+1} \right]_c$$

6. Pull back of stresses and tangent elastoplastic constitutive tensor to the reference configuration

$$^{n}(\mathbf{S})^{i+1} = \overset{\leftarrow}{\phi} \, ^{n}(\sigma)^{i+1}$$

$$^{n}(\mathbf{C})^{i+1} = \overset{\leftarrow}{\underset{\leftarrow}{\phi}} \, ^{n}(\mathbf{c})^{i+1}$$

7. Compute the residual force in the reference configuration and check convergence

$$^{n}\left[F_{\text{resid}}^{(e)} \right]^{i+1} \Rightarrow ^{n}(F_{\text{resid}})^{i+1} = \mathbb{A}_{e=1}^{\text{nelem}} \left[F_{\text{resid}}^{(e)} \right]^{i+1}$$

If $\|F_{\text{resid}}\| > 0? \Rightarrow i = i + 1$ Go back to (1)

else converged solution for the nth increment

$n = n + 1$ Compute new load increment

- END LOOP OVER EACH EQUILIBRIUM ITERATION
★ END LOOP OVER LOAD INCREMENTS
STOP

7. Numerical examples

7.1. General description

In this section application examples using the proposed model are presented. The examples consist in the numerical simulation of the non-linear behavior of a specimen made up of composite material subjected to a tension state. The simulations have been carried out using a finite element mesh of standard four node rectangular finite elements with 1988 elements, 2097 nodes and 4194 degrees of freedom. This mesh is similar to the one used in a study carried out by the European Space Agency [36]. (see Fig. 6a).

The test is carried out on specimens of carbon-epoxy T300/914C that present a notch in the central area of the specimen. The reinforcement are carbon fibers. The angle orientations of the carbon fibers in the different tests specimens are: 0°, 10°, 45° and 90° related to the longitudinal axis of the sample.

The test consists in a tensional state imposing a displacement on the top of the specimen. In Fig. 5 dimensions of the specimen, a detail of the central area and the points in which the experimental measures were carried out are observed.

In the notched area a stress concentration is generated which perturbs the matrix. This situation generates stresses that exceed the elastic limit of the matrix. In unidirectional fiber-reinforced composite materials cracks always start in the matrix and tend to advance parallel to the fiber direction. This behavior is the opposite to that observed in tests carried out on homogeneous isotropic specimens.

The resin behaves as an isotropic material with an elastoplastic constitutive law, while fibers behave as an anisotropic elastoplastic material [6].

In each numerical simulation the previously described constitutive model is used. The mechanical properties of each phase (matrix and fiber) are summarized in Tables 1 and 2. Numerical results presented can be divided in two groups:
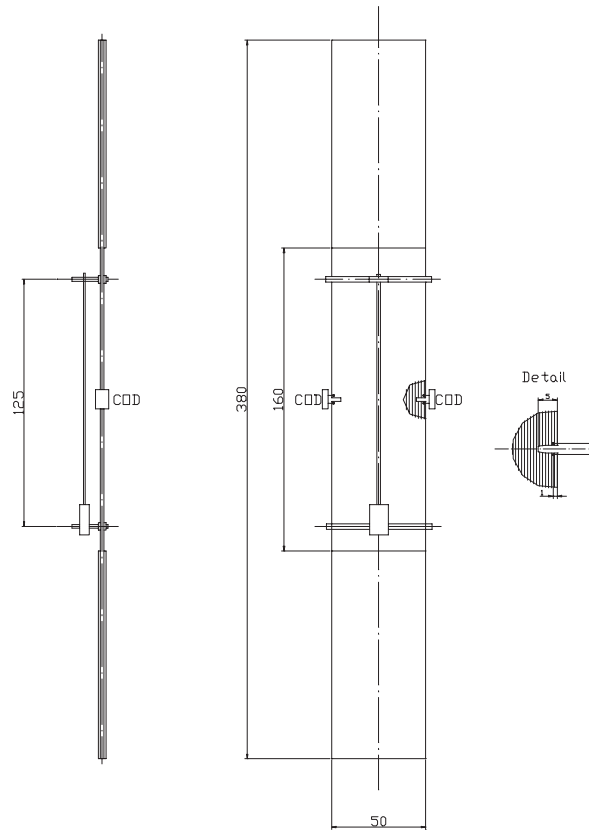
Fig. 5. Specimen geometry. Dimensions and detail of the central part.

Table 1
Material properties of epoxy resin

Young modulus	13,000 MPa
Poisson coefficient	0.325
Yield stress	43.323 MPa
Post yield behavior law	Exponential with softening
Fracture energy	5 N/m
V_m	52.5%

Table 2
Material properties of carbon fiber

Young modulus	239,551 MPa
Poisson coefficient	0.0
Yield stress	300 MPa
Post yield behavior law	Linear with hardening
V_f	47.5%

- Graphic results, in which the deformation of the specimen as well as iso-surfaces of the final stress, strain and equivalent plastic states are presented.
- Quantitative results, in which numerical X–Y curve are plotted and compared with experimental results. The experimental data have been obtained from the ESI Project Nb ED/83-383/RD/MS and ED/84-415/RD/MS and from a research project carried out by the European Space Agency [36].

7.2. Test of T300/914C specimens with 0° fiber angle

A sample of carbon epoxy with 0° fibers related to the longitudinal axis of the specimen is submitted to an imposed displacement on the top.

It is considered that the resin behaves as an isotropic Von Mises material with an elastoplastic behavior law. The mechanical properties of the epoxy resin are given in Table 1.

It is considered that the fiber behaves as an anisotropic elastoplastic material. The mechanical properties used in the numerical simulation are summarized in Table 2.

An incremental analysis considering 30 displacement increments was performed. The total displacement imposed at the top of the specimen was 0.385 mm.
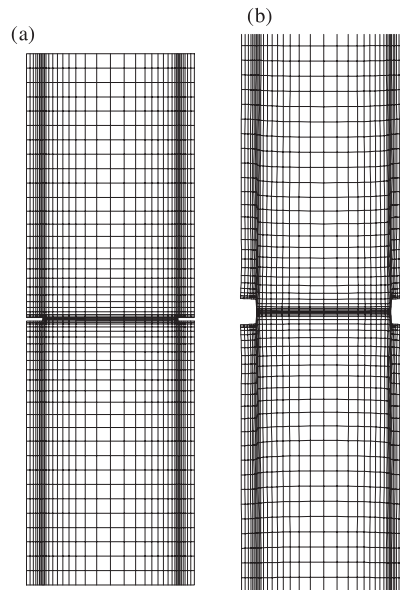
Fig. 6. (a) Finite element mesh used in numerical tests. (b) Test of T300/914C specimen with 0° fiber angle. Deformation (amplified 50 times).
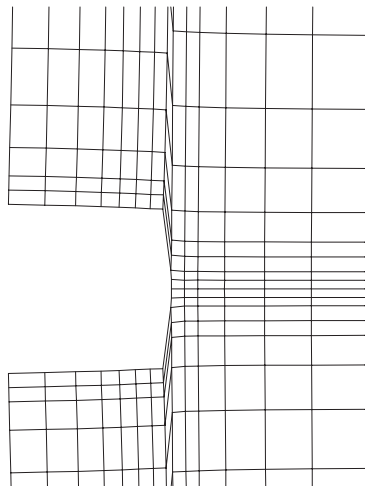
Fig. 7. Test of T300/914C specimen with 0° fiber angle. Detail of deformation at the notch.

Figs. 6b and 7 show the deformation of the specimen in the final state, and a detail of the deformation in the notched zone, respectively. These figures present a displacement amplification factor of 50 illustrating the most important phenomena obtained in the analysis.

In Fig. 6b is clearly observed that due to the vertical position of the carbon fibers the external faces of the specimen do not deviate from the vertical axis of the specimen. Deviation does take place when the fibers are inclined with respect to the longitudinal axis of the sample (see tests with fibers at 10° and 45°, Figs. 14 and 21a).

For the 0° case four cracks start in the notch root and progress parallel to the longitudinal axis of the specimen coincident with the reinforcement direction. The origin of two of the cracks can be appreciated in Fig. 7. They start in the notch root and spread in the direction of the longitudinal axis.

In Fig. 8a contours of the displacements norm are presented. It is observed that in the central area of the specimen the displacement field presents a soft gradient, with four areas clearly distinguished where displacement gradients are high. These areas begin in the root of each notch and progress parallel to the longitudinal axis of the specimen, coincident with the reinforcement direction.
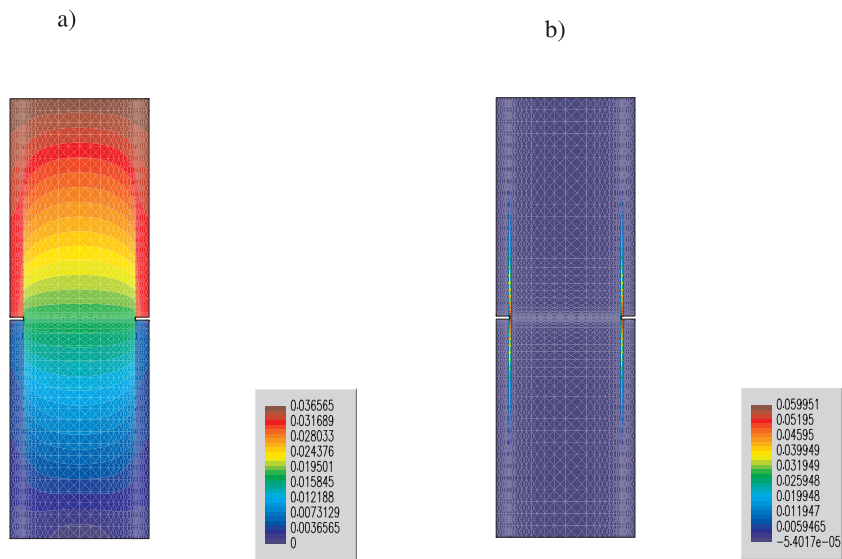
Fig. 8. Test of T300/914C specimen with 0° fiber angle: (a) Contours of displacement norm. (b) Equivalent plastic strain contours.
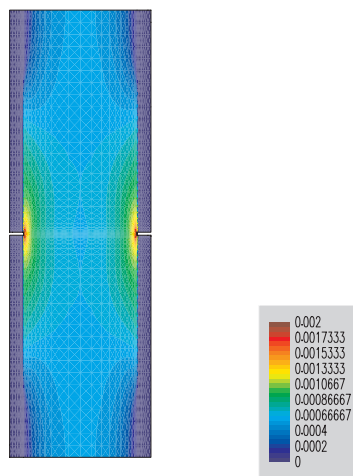
Fig. 9. Test of T300/914C specimen with 0° fiber angle. Contours of equivalent plastic strain in fibers.

The equivalent plastic strain contours in the composite are plotted in Fig. 8b. The areas with higher straining are in the notch root due to the concentration of stresses. Plasticity effects progress in a parallel direction to the longitudinal axis of the sample.

Fig. 9 shows the plasticity levels in fibers clearly indicating the regions where the debonding phenomenon has taken place. One of the reasons of the non-linear behavior of reinforced composite materials is due to the phenomenon of crack propagation in the matrix and the relative displacement between fiber and matrix. The phenomena of matrix cracking and debonding or slip between fibers and matrix reduce the global stiffness and leads to inelastic or not recoverable strains. This phenomenon is taken into account here by limiting the load capacity of the fibers due to the inability of the matrix to transmit the loads. More details about modeling of this phenomenon will be reported in a future work. Fig. 9 also clearly shows that cracks progress from the root of the notch, due to the concentration of stresses in this area, towards the center of the specimen. The debonding phenomenon prevents fibers reaching the maximum yield stress as the matrix
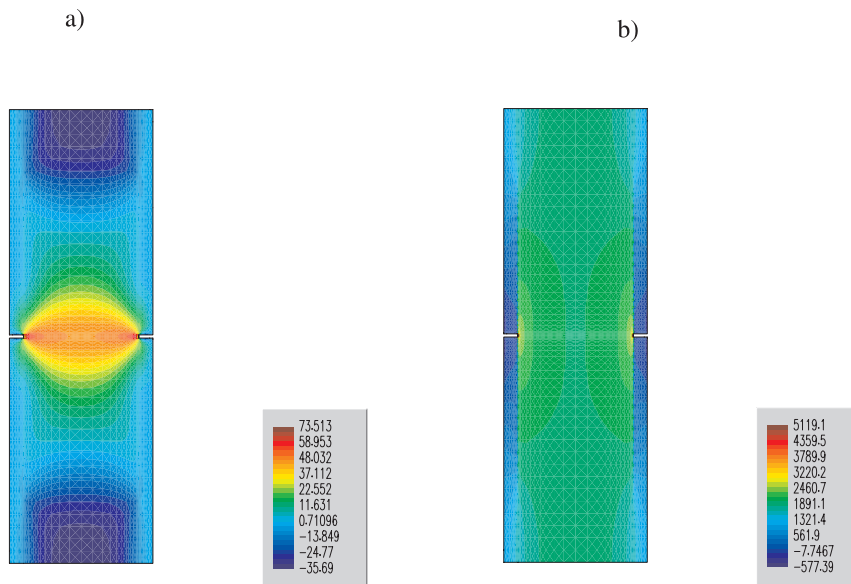
Fig. 10. Test of T300/914C specimen with 0° fiber angle. (a) Contour of σ_{xx} stress in the composite. (b) Contour of σ_{yy} stress in the composite.
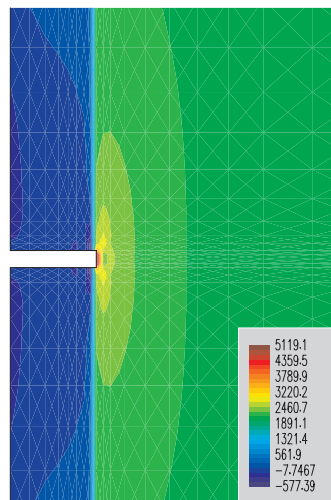
Fig. 11. Test of T300/914C specimen with 0° fiber angle. Detail of σ_{yy} stress contours at the notch.

is not able to transfer the load to the fiber. This also leads to a change in the slope of the load–displacement curve (Fig. 12).

In Figs. 10a and b contours of σ_{xx} and σ_{yy} stresses in the composite are plotted. The stress concentration in the notched area as well as the changes in the stress state taking place in the cracked area are shown.

In Fig. 11 a detail of the σ_{yy} stresses in the vicinity of the notched area is shown.

Some experimental and numerical results are compared in Figs. 12 and 13. The curve in Fig. 12 shows the force vs. the displacement at the top of the specimen. A comparison between experimental results, the results obtained with the mixing theory considering a linear elastic behavior for each phase and the proposed non-linear model is presented. Results using the linear elastic model provide upper limit values.

At high load levels a non-linear behavior is observed in experimental tests due to debonding phenomena between fibers and matrix. Numerical results detect with remarkable agreement the onset of this non-linear
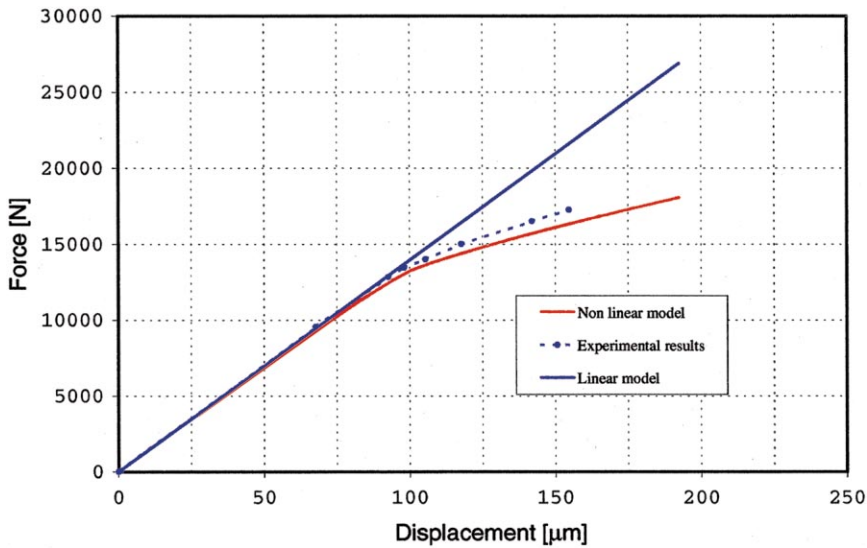
Fig. 12. Test of T300/914C specimen with 0° fiber angle. Load vs. displacement at the top of the specimen.
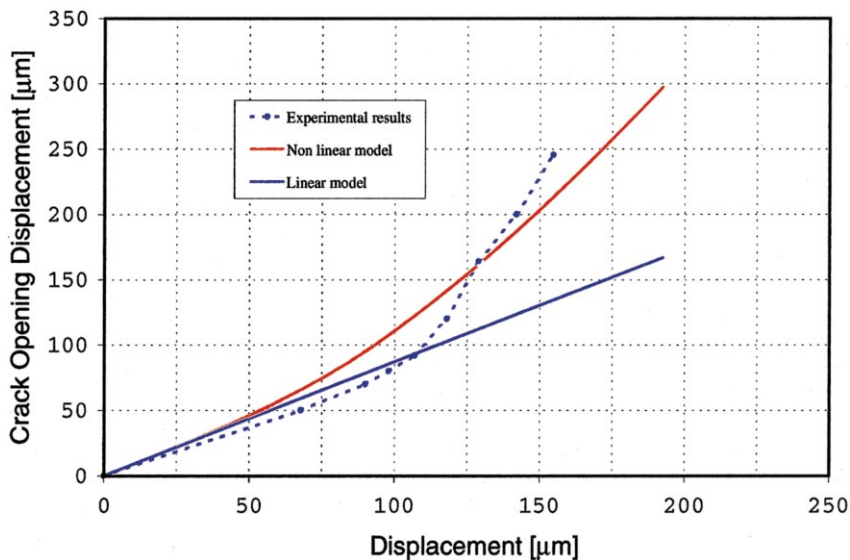
Fig. 13. Test of T300/914C specimen with 0° fiber angle. COD vs. displacement at the top of the specimen.

phenomenon. In Fig. 13 curves relating the displacement at the top level of the specimen and the crack opening displacement (COD) in the central area are plotted (see Fig. 5).

The overall agreement between experimental and numerical results obtained with the full non-linear model can be considered satisfactory.
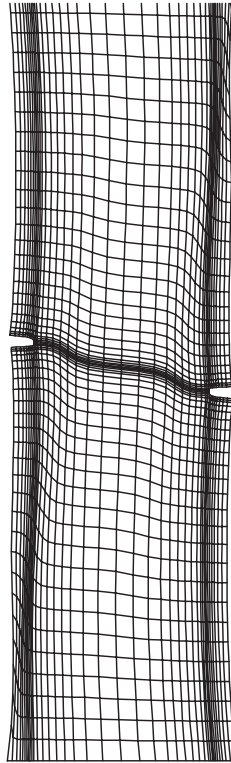
Fig. 14. Test of T300/914C specimen with 10° fiber angle. Deformation (amplified 30 times).

a)   b)
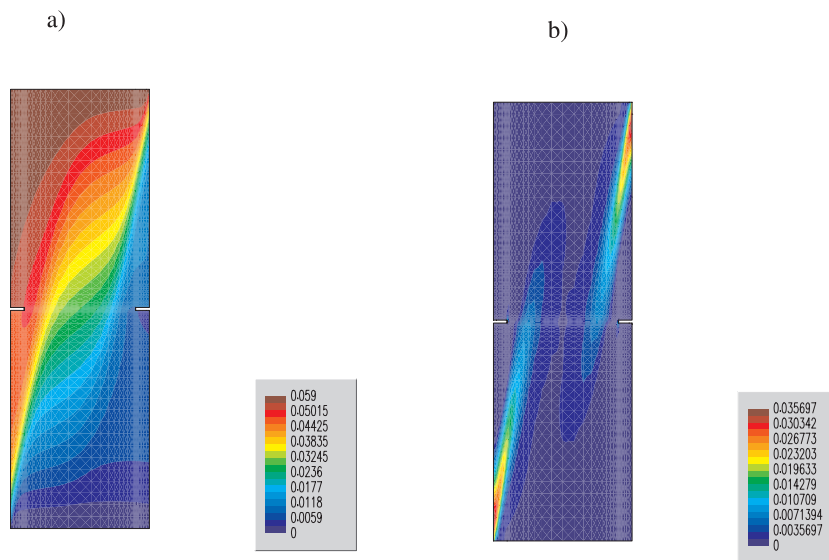
Fig. 15. Test of T300/914C specimen with 10° fiber angle: (a) Contours of displacement norm. (b) Equivalent plastic strain contours.

7.3. Test of T300/914C specimens with 10° fiber angle

The numerical simulations have been carried out considering a total of 50 time displacement increments. The total imposed displacement at the top level was 0.59 mm.

In Fig. 14 the deformed sample is presented. This figure presents an amplification factor of the displacements of 30 times. Note that due to the position of the carbon fibers, the external faces of the specimen deviate with the vertical axis of the sample. This phenomenon is due to a tendency of the fibers to be re-oriented in the direction of the applied force.

In Fig. 15a the displacements norm contours are plotted. In the same figure, it can be observed that the displacement field presents discontinuities in the central area of the specimen. In this region a crack starts along the reinforcement direction.

In Fig. 15b contours of the equivalent plastic strain are presented. Note the areas in which plastic straining has taken place. It is observed that due to the imposed displacement conditions, plastic straining
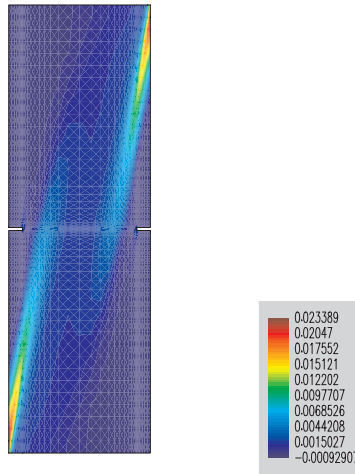
Fig. 16. Test of T300/914C specimen with 10° fiber angle. Contours of plastic deformation in the composite.
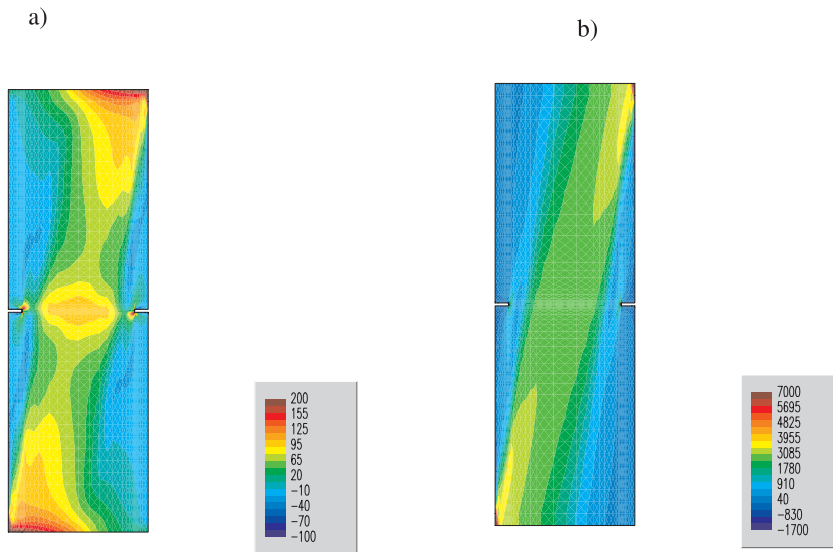
Fig. 17. Test of T300/914C specimen with 10° fiber angle: (a) Contour of σ_{xx} stress in the composite. (b) Contour of σ_{yy} stress in the composite.

takes place in the right upper part and the left lower zone of the specimen and it progress in a direction coincident with the reinforcement orientation.

Fig. 16 shows the plastic strains in the composite. It is observed that plastic strains take place in the right upper and left lower corner zones and progress towards the center of the specimen.

In Figs. 17a and b contours of σ_{xx} and σ_{yy} stresses are presented. An induced directionality is observed in the material.

The experimental and numerical results are compared in Figs. 18–20.

In this case analytical results present a good agreement with those obtained experimentally, except for the case of Fig. 19 in which a higher crack opening can be observed in the notched area on the right-hand side of the specimen. It is necessary to highlight that the experimental results do not show symmetry and the crack opening displacement is different at the left and right top sides. This could be due to measurement errors or discontinuities in the material. This phenomenon is not observed in the numerical simulation and
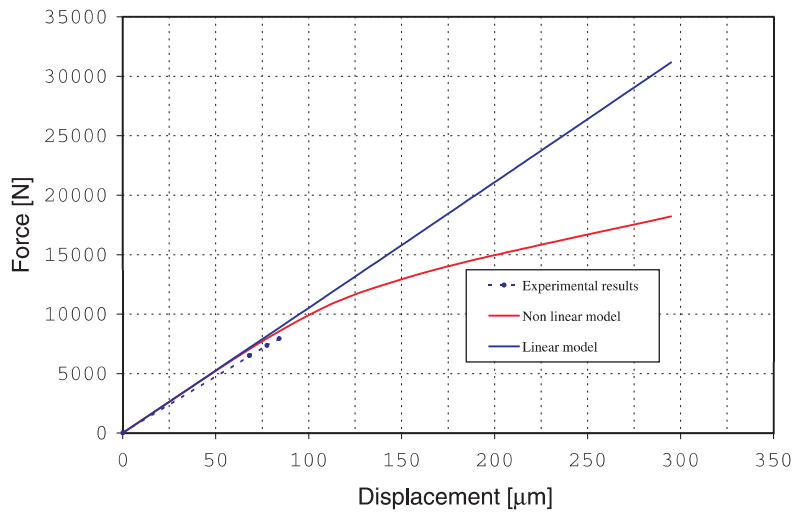
Fig. 18. Test of T300/914C specimen with 10° fiber angle. Load vs. displacement at the top of the specimen.
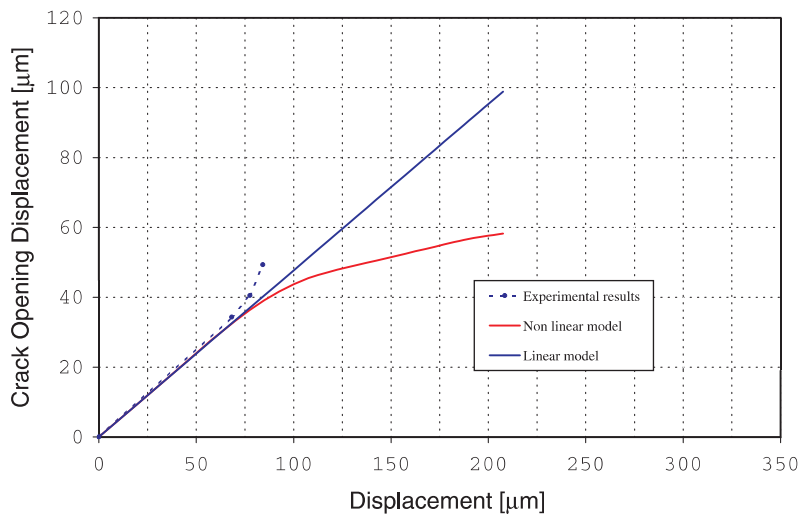
Fig. 19. Test of T300/914C specimen with 10° fiber angle. COD vs. displacement at the top of the specimen (right-hand side).
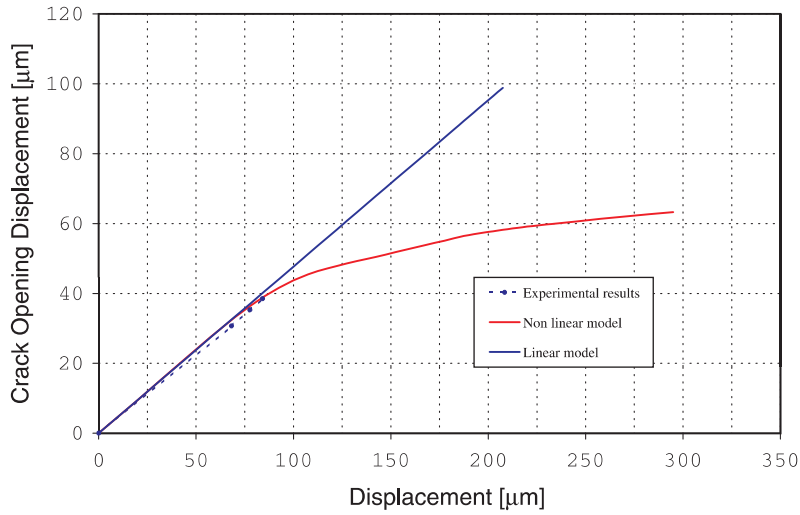
Fig. 20. Test of T300/914C specimen with 10° fiber angle. COD vs. displacement at the top of the specimen (left-hand side).

symmetric results have been obtained. The size of the crack opening displacements is the same for both top sides.

A comparison between numerical and experimental results for the right top side of the specimen is shown in Fig. 19. A non-gradual increase of the displacements field is observed in experimental results at the final stage of the test. In Fig. 20 numerical results agree well with experimental values.

7.4. Test of T300/914C specimens with 45° fiber angle

An incremental analysis has been performed with a total of 50 displacement increments. The total imposed displacement at the top level was 0.59 mm.
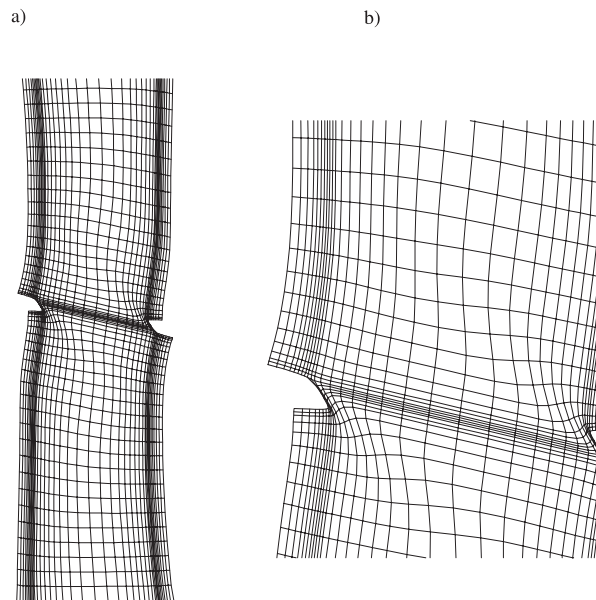
Fig. 21. Test of T300/914C specimen with 45° fiber angle: (a) Deformation (amplified 25 times). (b) Detail of deformation at the notch.

In Figs. 21a and b the deformed sample and a detail of the notched area are presented, respectively. These figures present a displacement amplification factor of 25 times. Note the rotations of the external faces due to the 45° direction of the reinforcement. This phenomenon takes place due to a tendency of the fibers to be reoriented in the direction of the applied force.

In Fig. 22a contours of the displacements norm are presented. Strain localization can be appreciated in the central area of the sample. This agrees with experimental results. Note that the cracks progress along the reinforcement direction.

In Fig. 22b contours of the equivalent plastic strain are observed. It is appreciated that plasticity is associated with the matrix materials and progresses normally to the reinforcement direction. This phenomenon takes place when the fibers try to align with the force direction. This produces changes in the stress field in the matrix generating plastic strains and debonding.

Fig. 23 shows the plasticity levels in the fibers clearly indicating the regions where the debonding phenomenon has taken place.

a)   b)
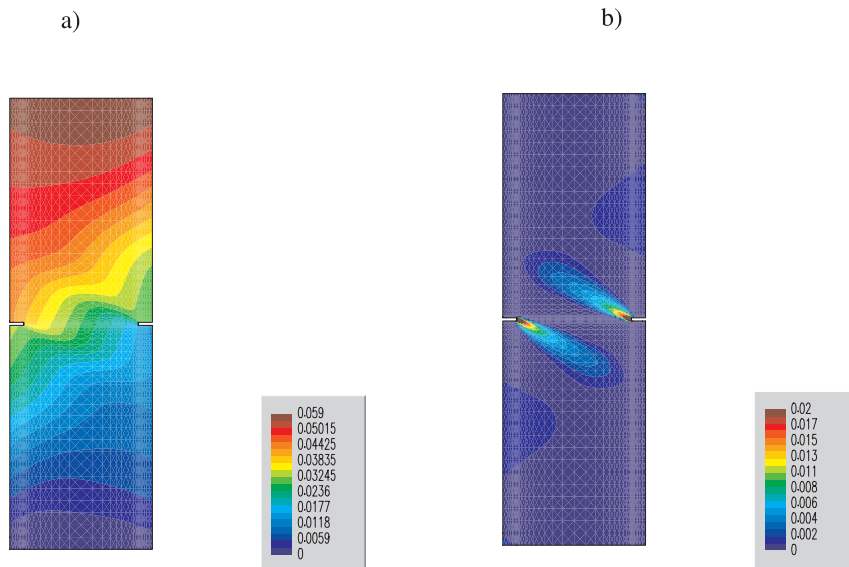
Fig. 22. Test of T300/914C specimen with 45° fiber angle: (a) Contour of displacement norm. (b) Equivalent plastic strain contours.
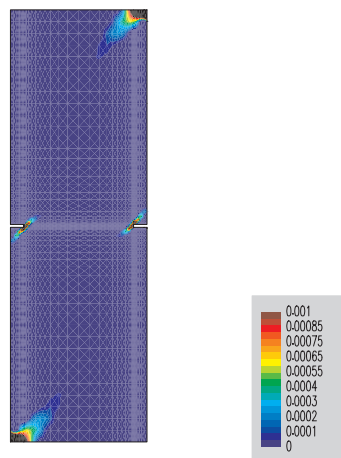
Fig. 23. Test of T300/914C specimen with 45° fiber angle. Contours of equivalent plastic strain in fibers.

In Figs. 24a and b contours of σ_{xx} and σ_{yy} stresses are presented. Again an induced directionality is observed in the material.

The experimental and numerical simulation results are observed in Figs. 25–27. As in previous cases experimental results are compared with those obtained numerically using the proposed non-linear model and a simpler model based on the mixing theory and assuming a linear behavior for both fiber and matrix.

Analytical results present a good agreement with experimental values in this case. Note the symmetry of the experimental results. This phenomenon is also observed in the numerical results and the values of the crack opening displacements are the same for both sides of the specimen (Figs. 26 and 27).

a)   b)
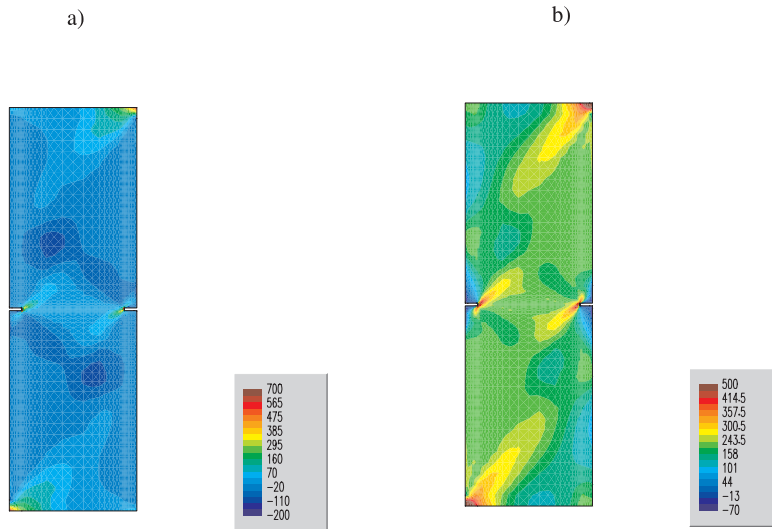
Fig. 24. Test of T300/914C specimen with 45° fiber angle: (a) Contour of σ_{xx} stress in the composite. (b) Contour of σ_{yy} stress in the composite.
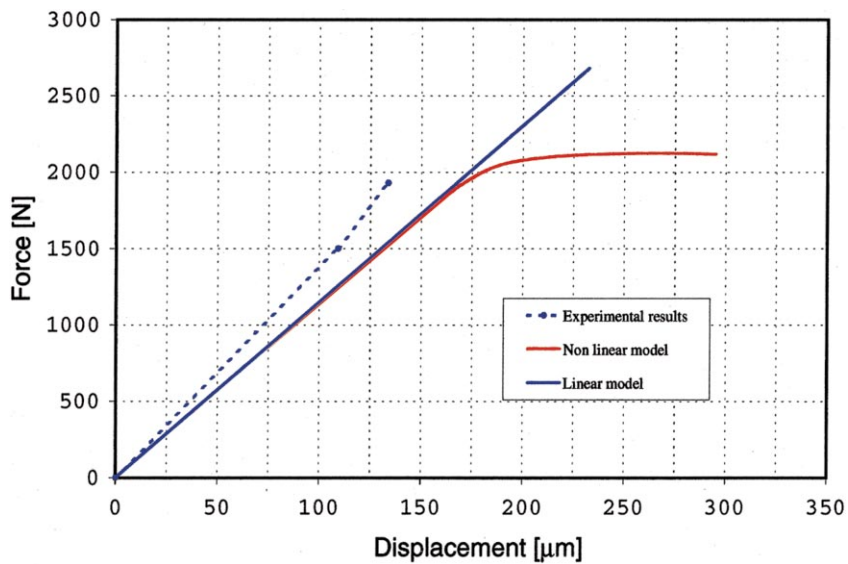
Fig. 25. Test of T300/914C specimen with 45° fiber angle. Load vs. displacement at the top of the specimen.
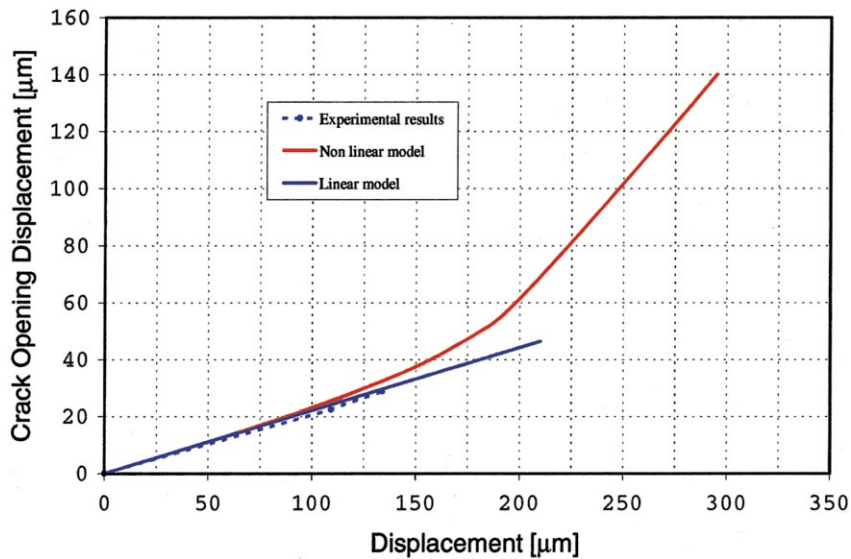
Fig. 26. Test of T300/914C specimen with 45° fiber angle. COD vs. displacement at the top of the specimen (right-hand side).
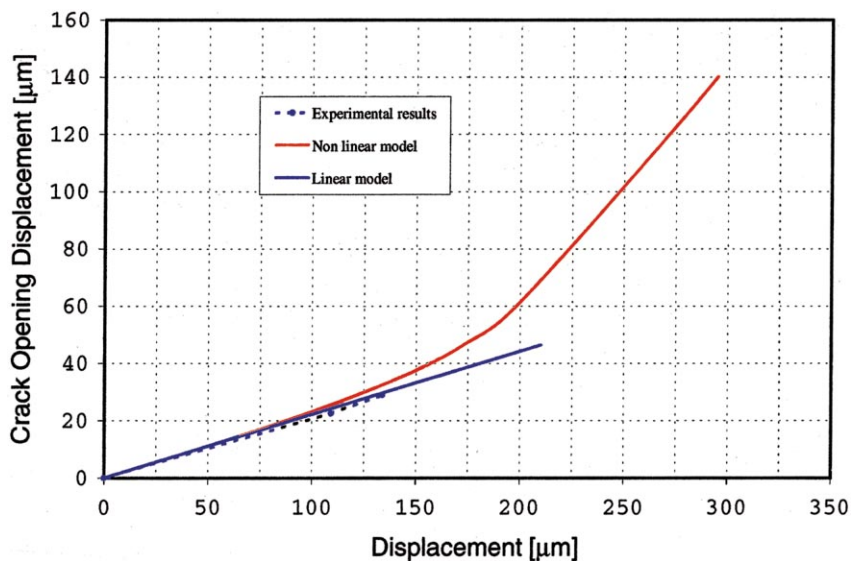
Fig. 27. Test of T300/914C specimen with 45° fiber angle. COD vs. displacement at the top of the specimen (left-hand side).

7.5. Test of T300/914C specimens with 90° fiber angle

An incremental analysis has been performed with a total of 40 displacement increment. The total imposed displacement at the top level was 0.385 mm.

In Fig. 28a and b the deformed sample and a detail of the notched area are presented. These figures present an amplification factor of the displacements of 200 times.

Fig. 28a shows the straining in the central area of the sample oriented in a perpendicular direction to the longitudinal axis, coincident with the direction of the reinforcement.

In Fig. 29a the displacements norm contours are plotted. In the same figure it can be observed that the displacement field presents discontinuities in the central area of the specimen. In this region a crack starts along the reinforcement direction.

a)   b)
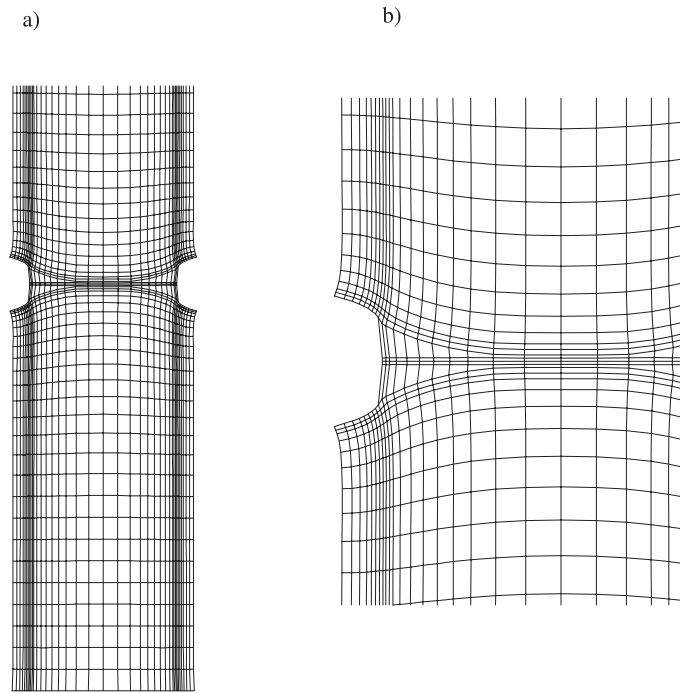
Fig. 28. Test of T300/914C specimen with 90° fiber angle: (a) Deformation (amplified 200 times). (b) Deformed detail at the notch.

a)   b)
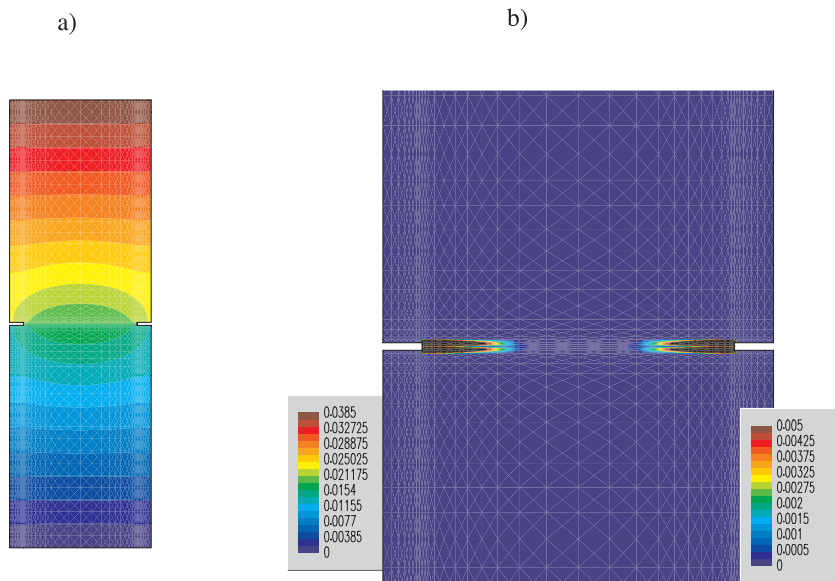
Fig. 29. Test of T300/914C specimen with 90° fiber angle: (a) Contours of displacement norm. (b) Detail of equivalent plastic strain contours at the notch.

In Fig. 29b contours of the plastic internal variable are shown. It can be appreciated that plastic strains start at the notch root and progress parallel to the reinforcement towards the center of the specimen.

In Figs. 30a and b contours of σ_{xx} and σ_{yy} stresses are plotted. In both figures the stress concentration due to the presence of the notch which generates plastic strains in the matrix can be appreciated.

The experimental and numerical simulation results are compared in Fig. 31. The curve shows the force vs. the displacement at the top of the specimen. The curve show the comparison between experimental

a)   b)
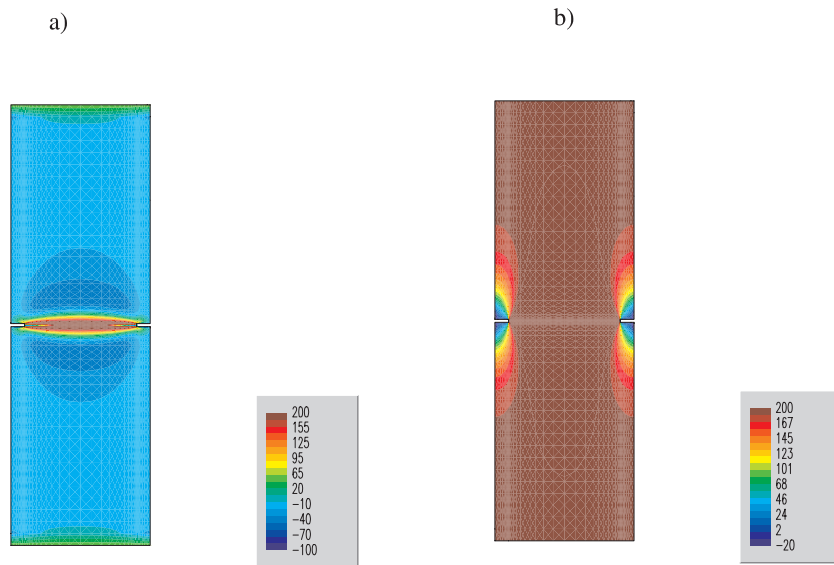
Fig. 30. Test of T300/914C specimen with 90° fiber angle: (a) Contour of σ_{xx} stress in the composite. (b) Contour of σ_{yy} stress in the composite.
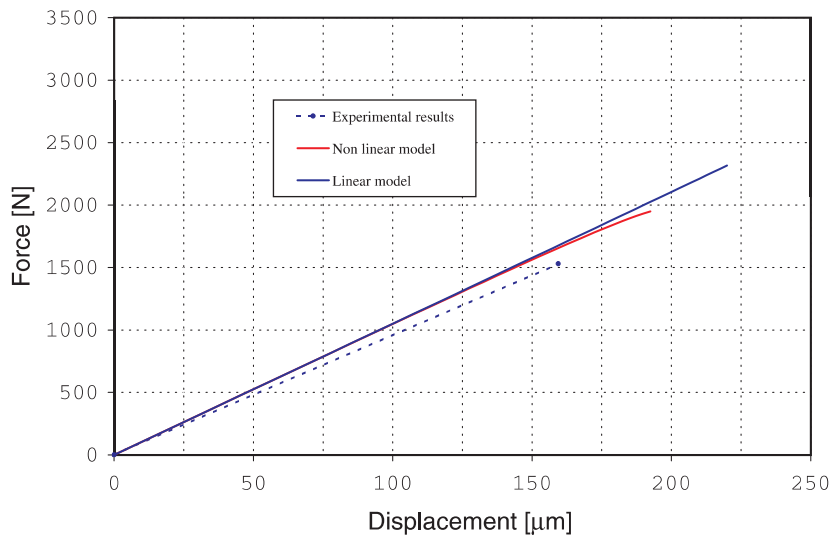
Fig. 31. Test of T300/914C specimen with 90° fiber angle. Load vs. displacement at the top of the specimen.

results, the results obtained with the mixing theory considering a linear elastic behavior for each phase and the proposed non-linear model. The numerical simulation using a linear elastic behavior gives the upper limit response as in previous examples.

8. Concluding remarks

The conventional techniques used for the analysis of simple isotropic materials are not valid for the non-linear analysis of composite materials.

In this work and as an alternative to more standard models the non-linear behavior of composite materials is modeled by means of a modified mixing theory, acting on a general anisotropic elastoplastic constitutive model formulated in large strains.

The use of an auxiliary fictitious isotropic space simplifies both the formulation of the non-linear constitutive model and the computational implementation into standard non-linear finite element codes.

The examples presented show that the constitutive model is appropriate for the analysis of composite materials in linear and non-linear regimes. The formulation is quite general and it allows to reproduce complex non-linear phenomena in composite materials such as anisotropy, large strains, plasticity and damage.

Acknowledgements

Appendix A. Transport operators

Objective derivative

$$L_\nu(\mathbf{x}) = \overleftarrow{\phi}\left[\frac{d}{dt}\left[\overrightarrow{\phi}(\mathbf{x})\right]\right]$$
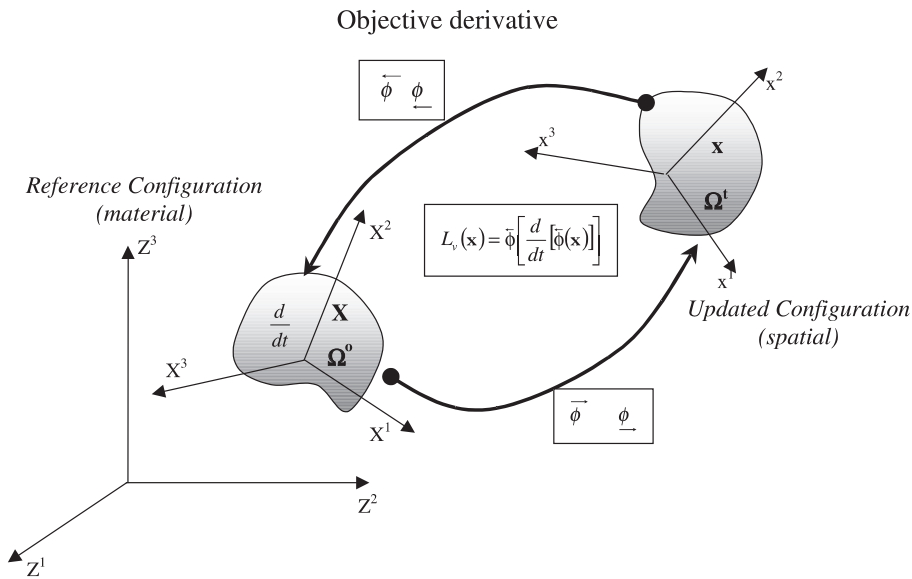
Concept of Lie's derivative

Operator	Index notation	Compact notation
$\mathbf{e} = \underset{\rightarrow}{\phi}(\mathbf{E})$	$e_{ij} = F_{iI}^{-T} E_{IJ} F_{jJ}^{-1}$	$\mathbf{e} = \mathbf{F}^{-T} \cdot \mathbf{E} \cdot \mathbf{F}^{-1}$
$\mathbf{E} = \underset{\leftarrow}{\phi}(\mathbf{e})$	$E_{IJ} = F_{iI}^{T} e_{ij} F_{jJ}$	$\mathbf{E} = \mathbf{F}^{T} \cdot \mathbf{e} \cdot \mathbf{F}$
$\sigma = \frac{1}{J}\overrightarrow{\phi}(\mathbf{S})$	$\sigma_{ij} = \frac{1}{J} F_{iI} S_{IJ} F_{jJ}^{T}$	$\sigma = \frac{1}{J}\mathbf{F} \cdot \mathbf{S} \cdot \mathbf{F}^{T}$
$\mathbf{S} = J\overleftarrow{\phi}(\sigma)$	$S_{IJ} = J F_{iI}^{-1} \sigma_{ij} F_{jJ}^{-T}$	$\mathbf{S} = J\mathbf{F}^{-1} \cdot \sigma \cdot \mathbf{F}^{-T}$
$\mathbf{c} = \underset{\rightarrow}{\overrightarrow{\phi}}(\mathbf{C})$	$c_{ijkl} = F_{iI} F_{jJ} F_{kK} F_{lL} C_{IJKL}$	
$\mathbf{C} = \underset{\leftarrow}{\phi}(\mathbf{c})$	$C_{IJKL} = F_{iI}^{-1} F_{jJ}^{-1} F_{kK}^{-1} F_{lL}^{-1} c_{ijkl}$	

References

[1] R. Ali, Use of finite element technique for the analysis of composite structures, Comput. Struct. 58 (5) (1996) 1015–1023.

[2] J. Betten, Creep theory of anisotropic solids, J. Rheol. 25 (1981) 565–581.

[3] J. Betten, Application of tensor functions to the formulation of yield criteria for anisotropic materials, Int. J. Plasticity 4 (1988) 29–46.

[4] E.L. Casas, S. Oller, J. Rubert, S. Proença, E. Oñate, A large strain explicit formulation for composites, in: S. Idelsohn, E. Oñate, E. Dvorkin (Eds.), Proceedings of the Fourth World Congress on Computational Mechanics, Buenos Aires, Argentina, CIMNE, Barcelona, Spain, 1998.

[5] M. Crisfield, Non-linear Finite Element Analysis of Solids and Structures, Wiley, New York, 1991.

[6] DFVLR, Progress letters on UD specimen tests, Technical report, European Space Agency, 1983.

[7] Engineering Systems International, The PAM-SCL code library, Engineering Systems International, Rungis-Cedex, France.

[8] C. Garcia Garino, J. Oliver, A numerical model for elastoplastic large strain problems, fundamentals and applications, in: D.R.J. Owen, E. Oñate, E. Hinton (Eds.), Computational Plasticity III, vol. 1, CIMNE, Barcelona, Spain, 1992, pp. 117–129.

[9] C. García Garino, J. Oliver, Use of large strain elastoplastic model for simulation of metal forming processes, Numer. Meth. Industrial Forming Processes (1992) 467–472.

[10] A. Green, P. Naghdi, A dynamical theory of interacting continua, J. Engrg. Sci. 3 (1965) 3–231.

[11] E. Haug, A. Kamoulakos, P.D. Luca, A.K. Pickett, Engineering models and their application to damage and forming simulation of composites, in: S. Idelsohn, E. Oñate, E. Dvorkin (Eds.), Proceedings of the Fourth World Congress on Computational Mechanics, Buenos Aires, Argentina, CIMNE, Barcelona, Spain, 1998.

[12] R. Hill, Micro mechanics of elastoplastic materials, J. Mech. Phis. Solids 13 (1965) 89–101.

[13] R. Hill, The Mathematical Theory of Plasticity, Oxford University Press, Oxford, 1971.

[14] D. Hull, An Introduction to Composite Materials, Cambridge University Press, Cambridge, 1987.

[15] J. Klintworth, S. Macmillian, Effective Analysis of Laminated Composite Structures, Benchmark, NAFEMS, 1992, pp. 20–22.

[16] E.W. Larson, Neutron transport and diffusion in inhomogeneous media, Nucl. Sci. Engrg. 60 (1976) 357–368.

[17] F. Len'e, Damage constitutive relations for composites materials, Engrg. Fract. Mech. 25 (1986) 713–728.

[18] F. Len'e, D. Leguilon, Homogeinized constitutive law for a partially cohesive composite material, Int. J. Solids Struct. 18 (1982) 443–458.

[19] J. Lubliner, Plasticity Theory, Macmillan, USA, 1990.

[20] B. Luccioni, S. Oller, R. Danesi, Coupled plastic-damage model, Comput. Meth. Appl. Mech. Engrg. 129 (1996) 81–90.

[21] L. Malvern, Introduction to the Mechanics of a Continuous Medium, Prentice-Hall, Englewood Cliffs, NJ, 1969.

[22] F.L. Matthews, R.D. Rawlings, Composite Materials: Engineering and Science, Chapman and Hall, London, 1994.

[23] E. Oñate, S. Oller, S. Botello, J. Canet, Methods for analysis of composite material structures (in Spanish), Technical Report 11, CIMNE, Barcelona, Spain, 1991.

[24] I.F. Obraztsov, V.V. Vasilev, Mechanics of Composites, Mir, Moscow, 1982.

[25] S. Oller, New ceramic materials for engineering structures (in Spanish), Technical Report 2, C.I.M.N.E, Barcelona, 1989.

[26] S. Oller, S. Botello, J. Miquel, E. Oñate, An anisotropic elastoplastic model based on an isotropic formulation, Engrg. Comput. 12 (3) (1995) 245–262.

[27] S. Oller, E. Oñate, J. Miquel, Simulation of anisotropic elastic–plastic behaviour of materials by means of an isotropic formulation, in Proceedings of the Second US National Congress on Computational Mechanics, Washington, DC, 1993a.

[28] S. Oller, E. Oñate, J. Miquel, S. Botello, A finite element model for analysis of multiphase composite materials, in: Proceedings of the Ninth International Conferences on Composite Materials , Zaragoza, Spain, Woodhead Publishing, 1993b.

[29] S. Oller, E. Oñate, J. Miquel, S. Botello, A plastic damage constitutive model for composite materials, Int. J. Solids and Struct. 33 (17) (1994) 2501–2518.

[30] B.P. O'Rourke, The use of composite materials in the design and manufacture of formula 1 racing cars, Proc. Inst. Mech. Engrg. C 387/025 (1989) 39–48.

[31] M. Ortiz, E. Popov, A physical model for the inelasticity of concrete, Proc. Roy. Soc. London A 383 (1982) 101–125.

[32] M. Ortiz, E. Popov, Plain concrete as a composite material, Mech. Mater. 1 (1982) 139–150.

[33] R. Pendleton, M. Tuttle, Manual on Experimental Methods for Mechanical Testing of Composites, Elsevier, Amsterdam, 1989.

[34] E. Sanchez Palencia, Non-homogeneous media and vibration, Lecture Notes in Physics, Springer, Berlin, 1980.

[35] J. Simo, R. Taylor, Consistent tangent operators for rate-dependent elastoplasticity, Comput. Meth. Appl. Mech. Engrg. 48 (1985) 101–118.

[36] C. Stavrinidis, Employment of Pam-Fiss Bi-Phase Computer Program for the Strength Analysis and Fracture Delamination Behaviour of Composites, vol. 7, Final Synthesis Report, Technical report, European Space Agency, 1985.

[37] P. Suquet, Méthodes d'homogénésation en mécanique des solids in comportements rhéologiques et structures de matériaux, Presses de L'ENPC, París, 1981, pp. 87–128.

[38] P. Suquet, Plastcité et Homogeneisation, Ph.D. Thesis, Université Pierre et Marie Curies, Paris, 1982.

[39] C. Trusdell, R. Toupin, The Classical Field Theories, Handbuch der Physik III/I, Springer, Berlin, 1960.